Supplementary figures

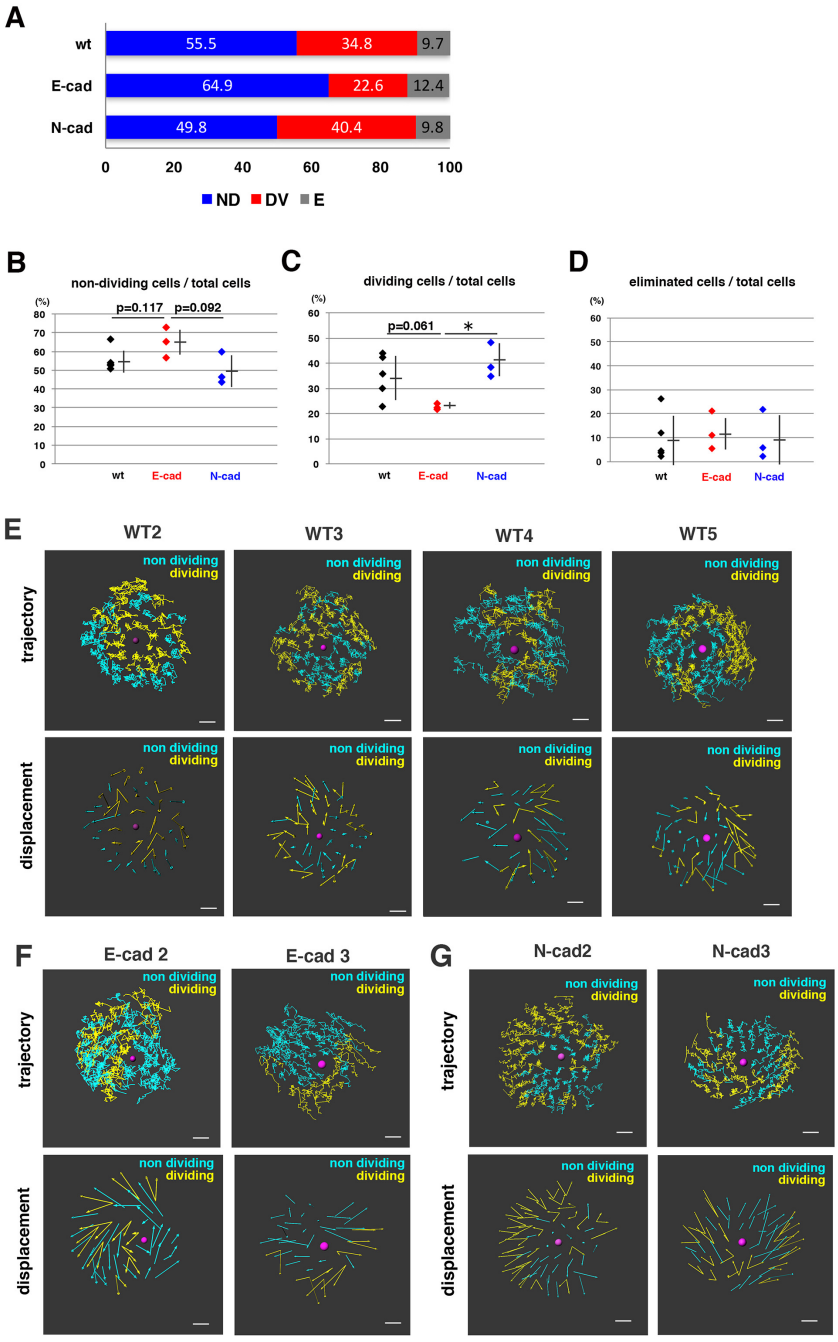

Figure S1. Fraction of non-dividing, dividing and eliminated cell populations in wild-type, E-cadherin mutant and N-cadherin morphant lenses

(A) Histogram of mean percentages of non-dividing (ND, blue), dividing (DV, red) and eliminated (E, grey) cell populations in five wild-type, three E-cadherin mutant, and three N-cadherin morphant lenses at 33 hpf. The fraction of dividing cell population was lower in E-cadherin mutant than in wild-type and N-cadherin morphant lenses.

(B–D) Fractions of non-dividing (B), dividing (C) and eliminated (D) cell populations in the anterior lens epithelium of the wild type, the E-cadherin mutant and the N-cadherin morphant at 33 hpf. Values for five wild-type, three E-cadherin mutant and three N-cadherin morphant lenses are plotted. Means and standard deviations are indicated by horizontal bars and vertical lines, respectively. Probabilities are calculated using Student's *t*-test: *p<0.05. In the case that probabilities are 0.05<p<0.15, p-values are indicated. The fraction of dividing cell population was lower in E-cadherin mutant than in wild-type and N-cadherin morphant lenses, although the difference between wild-type and E-cadherin mutant lenses was less significant (p=0.061 in (C)).

(E–G) Cell movement trajectory and displacement of additional four wild-type (E), two E-cadherin mutant (F), and two N-cadherin morphant lenses that we analyzed in this study. Scale bars: 10 μm.

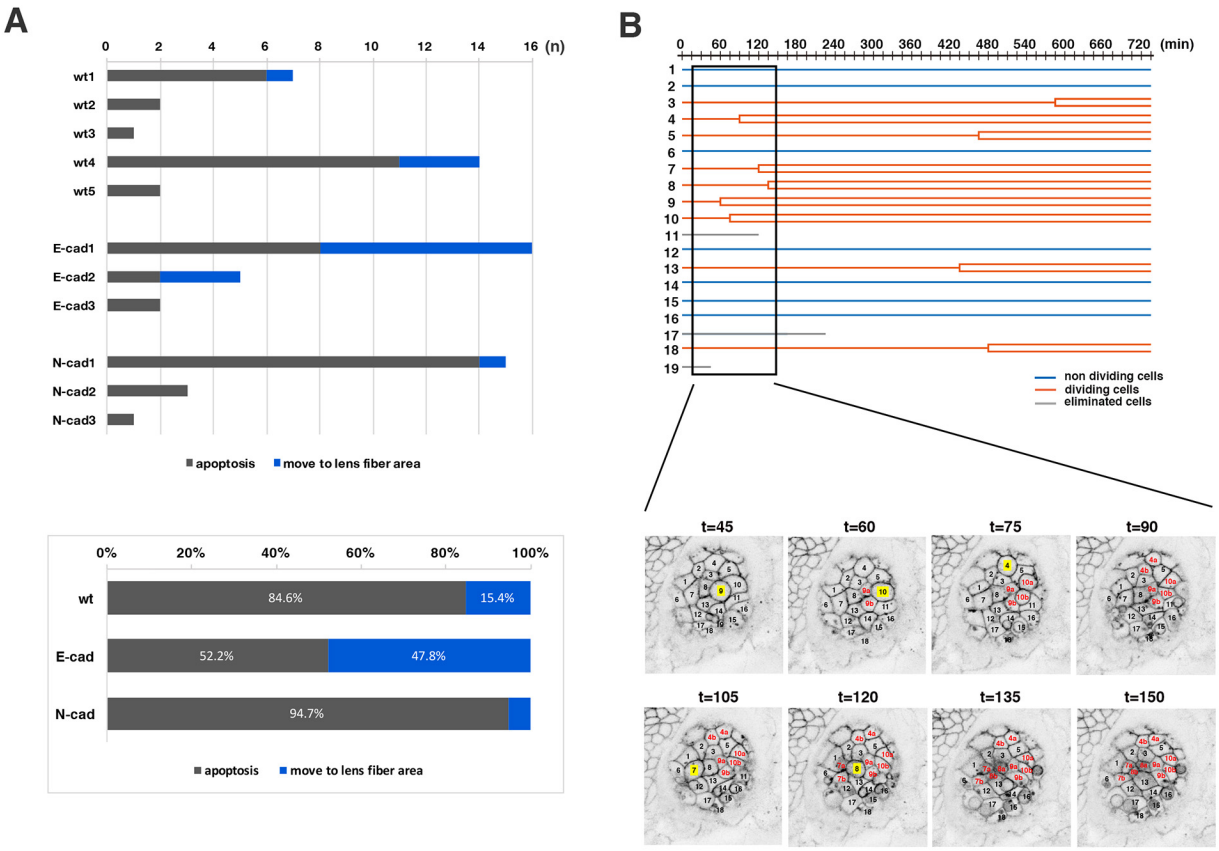

Figure S2. Analyses of the eliminated cell population and clustered cell divisions of wild-type lenses

(A) (Upper panel) Number of two types of eliminated cell population, which underwent apoptosis (grey) and moved into the lens fiber area (blue), respectively, in individual wild-type, E-cadherin mutant, and N-cadherin morphant lenses. The number of eliminated cells were varied depending on individual lenses. Eliminated cells that moved into the lens fiber area were generally observed in lenses with a high number of eliminated cells. (Lower panel) Histogram of the percentages of two types of eliminated cell population, which underwent apoptosis (grey) and moved into the lens fiber area (blue), respectively, relative to the total number of eliminated cells observed in five wild-type, three E-cadherin mutant, and three N-cadherin morphant lenses. The fraction of eliminated cells that moved into the lens fiber area was higher in E-cadherin mutant lenses (47.8%) than in wild-type lenses (15.4%), suggesting that E-cadherin suppresses cell movement from lens epithelium into the lens fiber area. In N-cadherin morphant lenses, this fraction was only 5.3%, much less than in wild-type lenses (15.4%).

(B) (Upper panel) Lineages of lens epithelial cells from zebrafish transgenic line, *Tg(h2afva:GFP; EF1α:mCherry-CAAX)* from 33 to 45 hpf, also shown in Movie2. Red, blue, and grey lines indicate dividing, non-dividing, and eliminated cell populations, respectively. (Lower panel) Confocal images for 135 min shown as squares in the upper panel. Only mCherry-CAAX fluorescence is shown. Numbers on individual cells correspond to cell numbers in the upper panel. Yellow squares and red numbers indicate mitotic cells and their daughter cells, respectively.

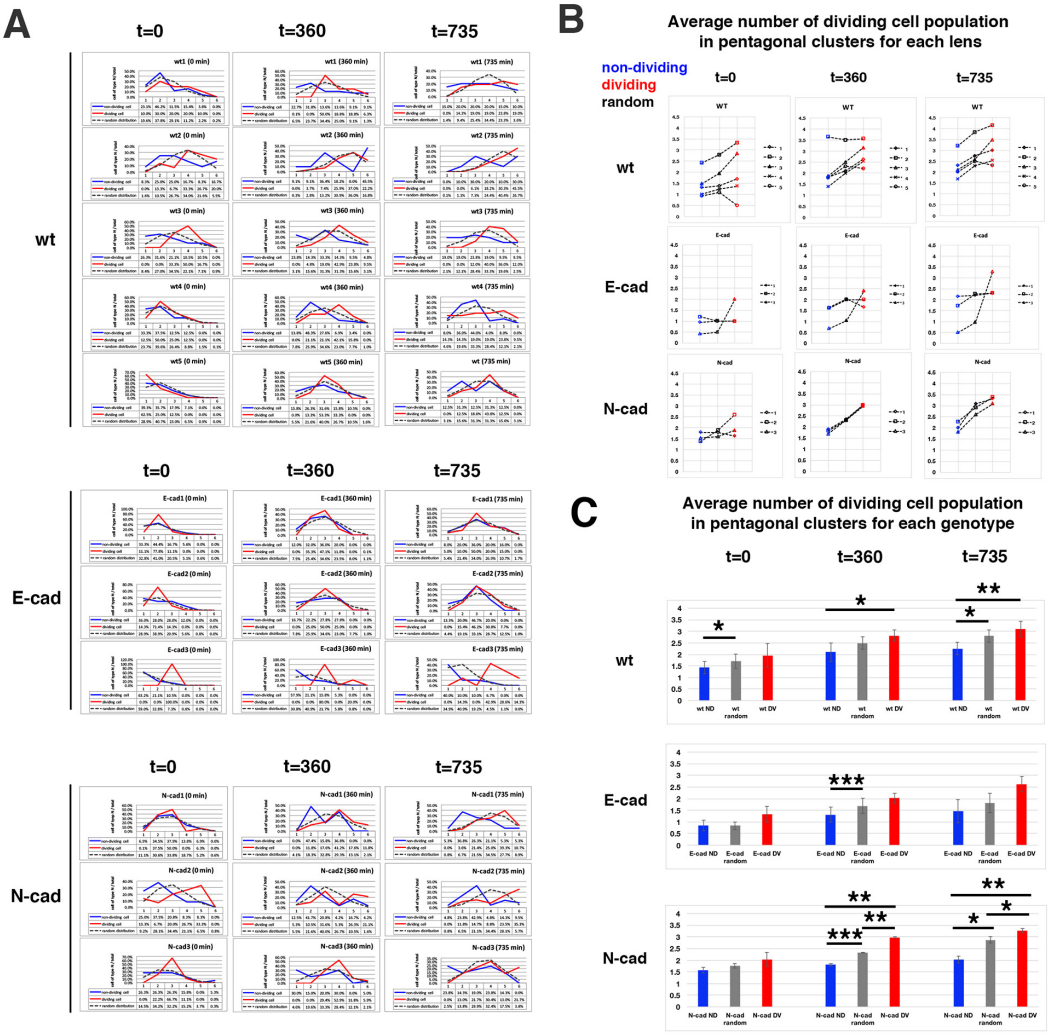

Figure S3. Analyses of non-dividing and dividing cell population clusters

(A) Distribution of pentagonal patterns of five wild-type, three E-cadherin mutant, and three N-cadherin morphant lenses during the scanned period. Times indicate the time elapsed after 33 hpf. Data at the end of the scanned period (t=735 min) are also shown in Figs. 1E, 3C, and 4C. Grey dotted lines indicate the profile of pentagonal patterns when non-dividing and dividing cell populations are randomly selected, whereas red and blue solid lines indicate the profiles of pentagonal patterns, in which cells pre-designated as dividing and non-dividing cell populations are in the center. Although distribution profiles were variable depending on individual lenses, distribution profiles of non-dividing and dividing cell population-centered pentagonal clusters were similar to that of random distribution model at t=0 in three of five wild-type lenses, two of three E-cadherin mutant lenses, and two of three N-cadherin morphant lenses. Non-dividing and dividing cell populations were gradually segregated to form clusters during development in wild-type and N-cadherin morphant lens epithelium. However, such segregation did not occur in lens epithelium of two E-cadherin mutant lenses, E-cad1 and E-cad2, during the scanned period. In one E-cadherin mutant lens, E-cad3, the distribution profile of dividing cell population-centered pentagonal clusters was strongly segregated from that of the random distribution model even at t=0, probably because dividing cells were extremely localized in the peripheral region (see Fig. S1F).

(B) Average number of dividing cell population in pentagonal clusters of each of wild-type, E-cadherin mutant and N-cadherin morphant lenses. In wild-type and N-cadherin morphant lenses, values of dividing and non-dividing cell population-centered pentagonal clusters gradually became higher and lower than those of random distribution model, respectively during the scanned period. However, in E-cadherin mutant lenses, two lenses showed similar numbers of non-dividing and dividing cell population-centered pentagonal clusters compared to the random distribution model at t=360 and 735, suggesting that segregation of non-dividing and dividing cell populations does not proceed normally in E-cadherin mutant lenses.

(C) Average number of dividing cell population in pentagonal clusters of five wild-type, three E-cadherin mutant, and three N-cadherin morphant lenses. Bar indicates standard error. Student's *t*-test: *p<0.05, **p<0.01, ***p<0.001. Significant differences between non-dividing cell population-centered clusters and dividing cell population-centered clusters were observed in wild-type and N-cadherin morphant lenses at 360 and 735 min. Furthermore, segregation between random distribution and non-dividing/dividing cell populations-centered clusters was enhanced in N-cadherin morphant lenses. On the other hand, there were no significant difference between non-dividing cell population-centered clusters and dividing cell population-centered clusters in E-cadherin mutant lenses.

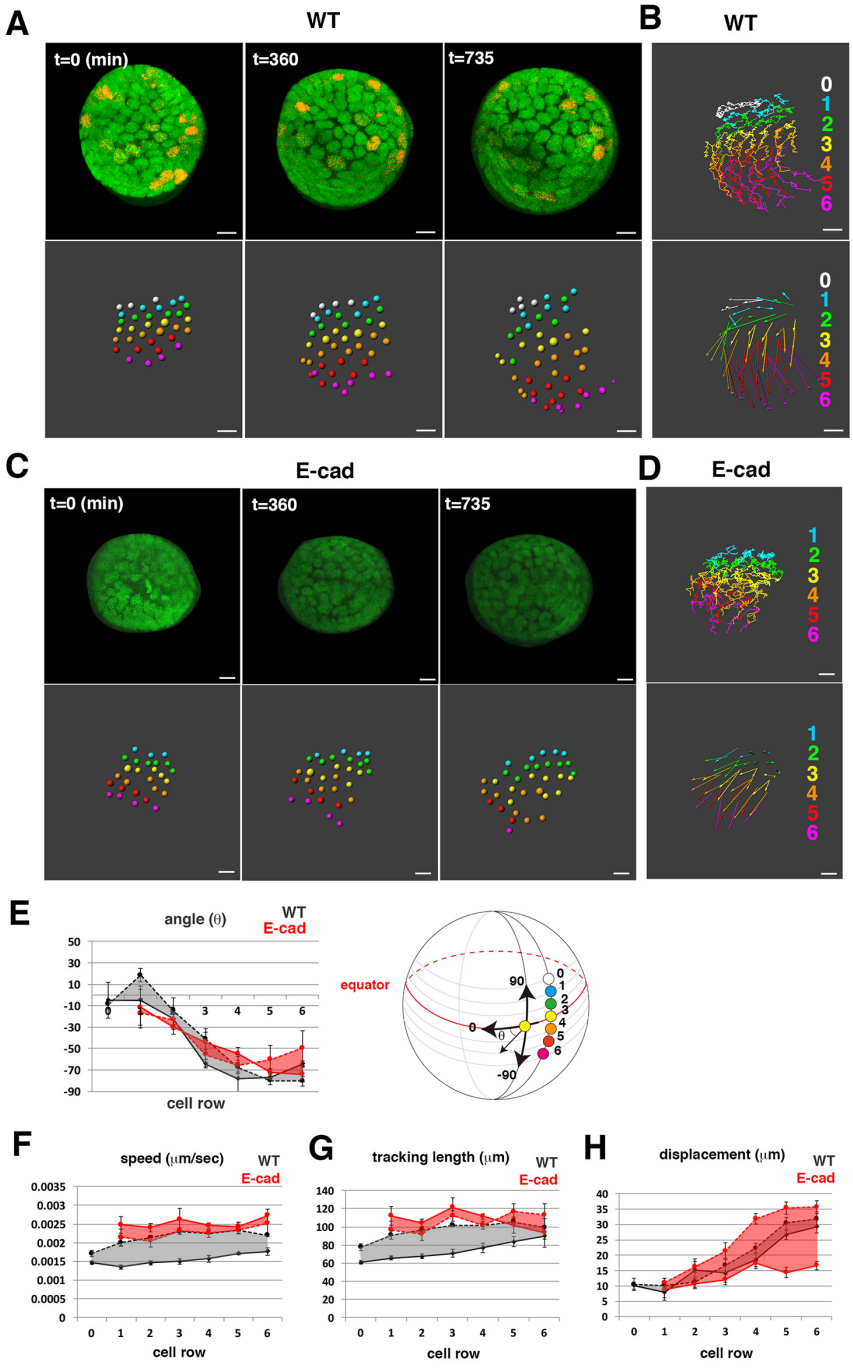

Figure S4. Cell movement in the equatorial region of the wild-type and the E-cadherin mutant

(A, C) Confocal images (upper) and nuclear positions (lower) in the equatorial region of wild-type (A) and *hab*^{rk3} mutant (C) lenses combined with *Tg(h2afva:GFP; EF1α:mCherry-zGem)*. Times elapsed after 33 hpf are indicated.

(B, D) Trajectory (upper) and displacement (lower) of cell movement in the equatorial region of wild-type (B) and *hab*^{rk3} mutant (D) lenses.

(E) Cell movement direction in the equatorial region of two wild-type (black) and *hab*^{rk3} mutant (red) lenses. Solid lines indicate the lens shown in (A–D). The zone between two lenses is indicated in color. The right panel indicates the definition of cell movement direction (θ).

(F–H) Speed (F), tracking length (G) and displacement (H) of cell movement in the equatorial region of two wild-type (black) and *hab*^{rk3} mutant (red) lenses. Solid lines indicate the lens shown in (A–D). The zone between two lenses is indicated in color.

Error bars indicate the standard error of the mean. Scale: 10 μm (A-D).

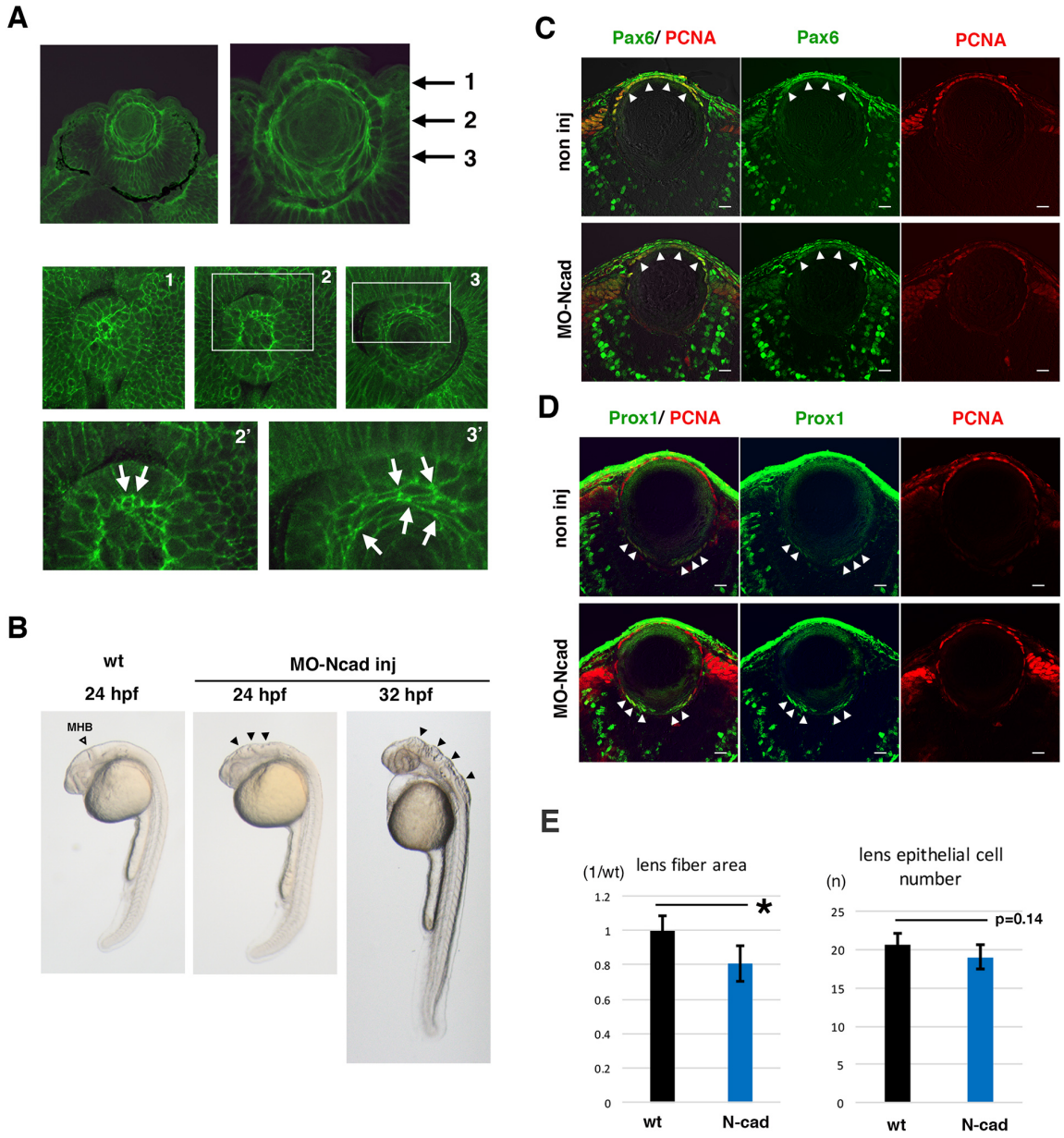

Figure S5. Lens fiber growth defects in an N-cadherin morphant

(A) Immuno-labeling of zebrafish lens with anti-N-cadherin antibody. The top two panels show sections of the retina and lens at 33 hpf. The middle three and bottom two panels show confocal scanning of horizontal planes in whole mount lens at 27 hpf. Three planes perpendicular to the AP axis, which contain the apical lens fiber suture (plane 1), the equatorial area (plane 2), and elongating lens fiber cells (plane 3), are shown in panels 1, 2, and 3, respectively. The bottom two panels indicate higher magnification images of white squares shown in panels 2 and 3. N-cadherin protein is markedly accumulated in plasma membrane of apical tips (arrows in panel 2') and the intermediate flattened region (arrows in panel 3') of lens fiber cells. These data suggest that N-cadherin is strongly expressed in elongating lens fiber cells.

(B) Morphology of N-cadherin morphant embryos at 24 and 32 hpf. The open arrowhead indicates the position of the midbrain-hindbrain boundary (MHB) in wild-type 24 hpf embryos. Black arrowheads indicate the failure of neural tube closure around the MHB in N-cadherin morphant embryos at 24 and 32 hpf.

(C–D) Labeling of wild-type and N-cadherin morphant lenses with antibodies against PCNA (red, C and D), Pax6 (green, C) and Prox1 (green, D). In the N-cadherin morphant, lens epithelial cells and differentiating lens fiber cells normally express Pax6 (arrowheads, C) and Prox1 (arrowheads, D), respectively.

(E) Histogram of lens fiber area size (left) and the number of lens epithelial cells (right) in wild-type (black) and N-cadherin morphants (blue). Six independent lenses for 72 hpf wild-type and N-cadherin morphant embryos were used to measure lens fiber area size with Image-J and to count lens epithelial cells on plastic sections that cover the central region of the lens sphere. The standard deviation is indicated. Student's *t*-test; * $p<0.05$. Scale: 10 μm (C, D).

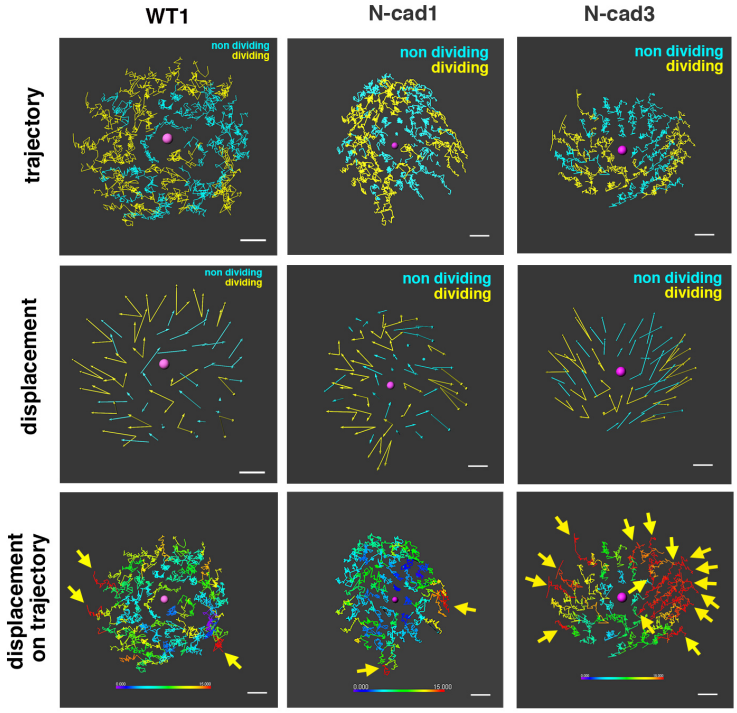

Figure S6. Analyses of cell movement in the anterior lens epithelium of an N-cadherin morphant
Trajectory (upper panels) and displacement (middle panels) of lens epithelial cells in wild-type, namely WT1, and N-cadherin morphant lenses, namely N-cad1 and N-cad3. The N-cad1 lens above is also shown in Figure 3. Blue and yellow colors indicate non-dividing and dividing cell populations, respectively. In the N-cad3 lens, the dividing cell population was unevenly located in the anterior epithelium. (Bottom panels) Displacement length shown in the trajectory of lens epithelial cells. The color range from blue to red corresponds to displacement length from low (0 μm) to high (15 μm), respectively. WT1, N-cad1, and N-cad3 lenses are shown. Yellow arrows indicate cells with longer displacements (>15 μm, red). The WT1 and N-cad1 lenses have a few long-displacement cells only in the peripheral region, whereas the N-cad3 lens has 15 long-displacement cells. Scale: 10 μm.

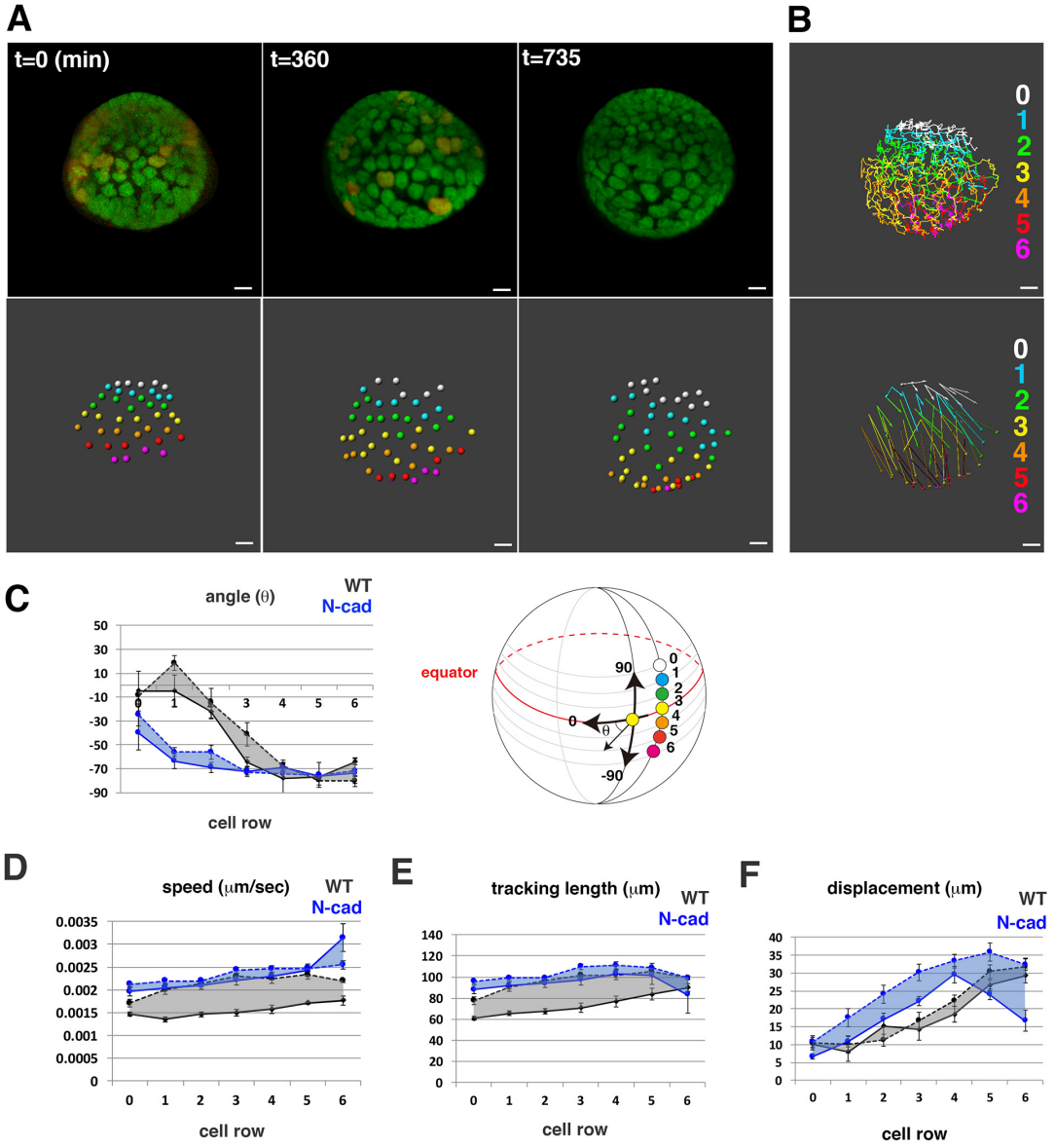

Figure S7. Cell movement in the equatorial region of an N-cadherin morphant

(A) Confocal images (upper) and nuclear positions (lower) of the equatorial region of an N-cadherin morphant lens combined with *Tg(h2afva:GFP; EF1α:mCherry-zGem)*. Time elapsed after 33 hpf is indicated.

(B) Trajectory of cell movement (upper) and cell displacement (lower) in the equatorial region of an N-cadherin morphant.

(C) Cell movement direction in the equatorial region of two wild-type (black) and N-cadherin morphant (blue) lenses. Solid lines indicate the lens shown in (A–B). The zone between two lenses is colored.

(D–F) Speed (D), tracking length (E) and displacement (F) in the equatorial region of two wild type (black) and N-cadherin morphant (blue) lenses. Solid lines indicate the lens shown in (A–B). The zone between two lenses is indicated in color. Error bars indicate the standard error of the mean. Scale: 10 μm (A–B).

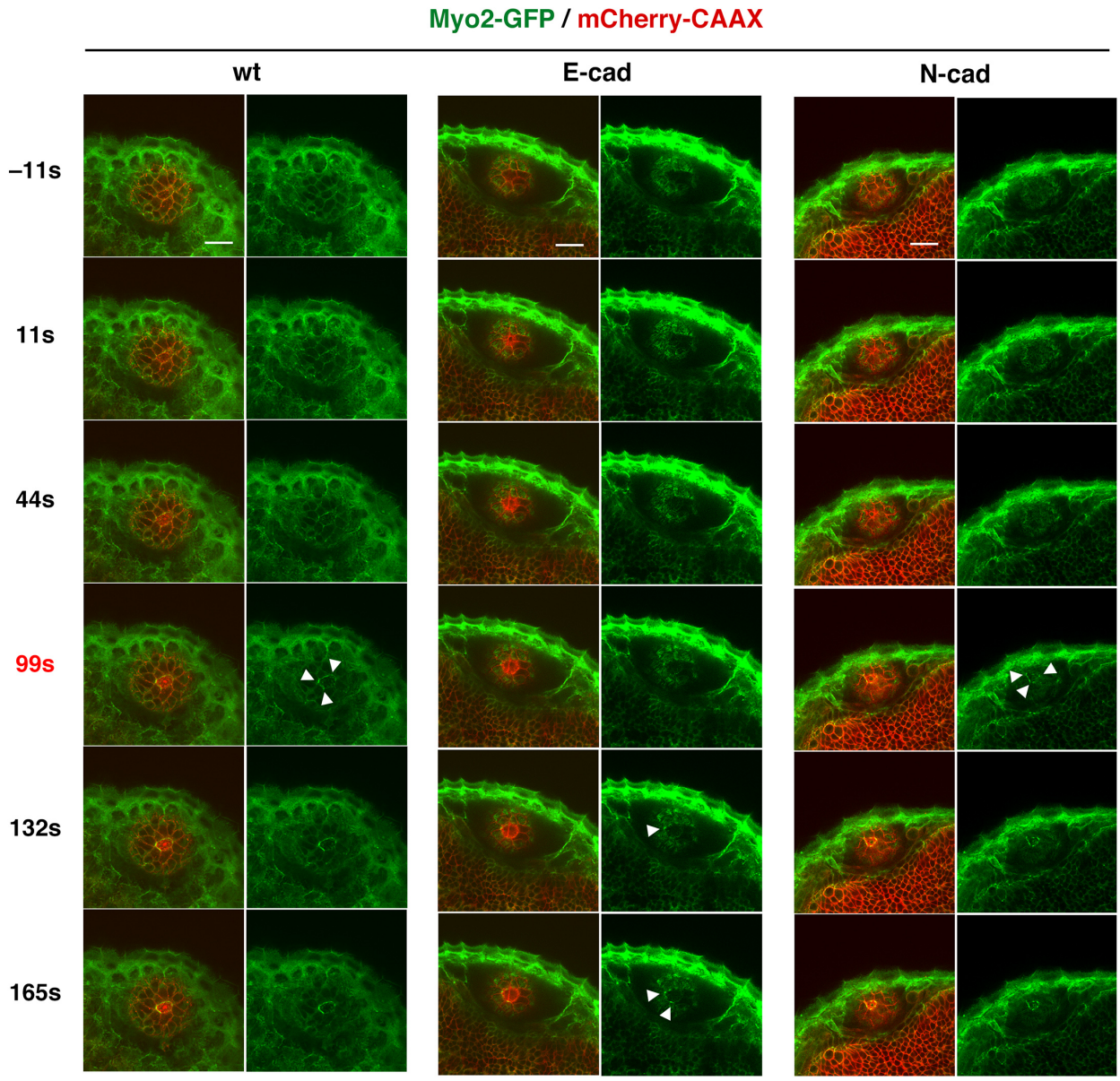

Figure S8. Analyses of Myosin2 accumulation in response to laser ablation
Time-lapse scanning of 50 hpf wild-type, E-cadherin, and N-cadherin morphant lens epithelia expressing *Tg(actb1:myl12.1-eGFP; EF1α: mCherry-CAAX)* after laser ablation. The right columns indicate only the green channel (Myosin 2). White arrowheads indicate accumulation of Myosin2 in cell membranes surrounding the ablated area. Myosin2 accumulated in all cases: wild-type, E-cadherin and N-cadherin morphant lenses, although accumulation was delayed in E-cadherin morphant lenses and occurred irregularly in patches in both E- and N-cadherin morphant lenses. Scale: 20 μm.

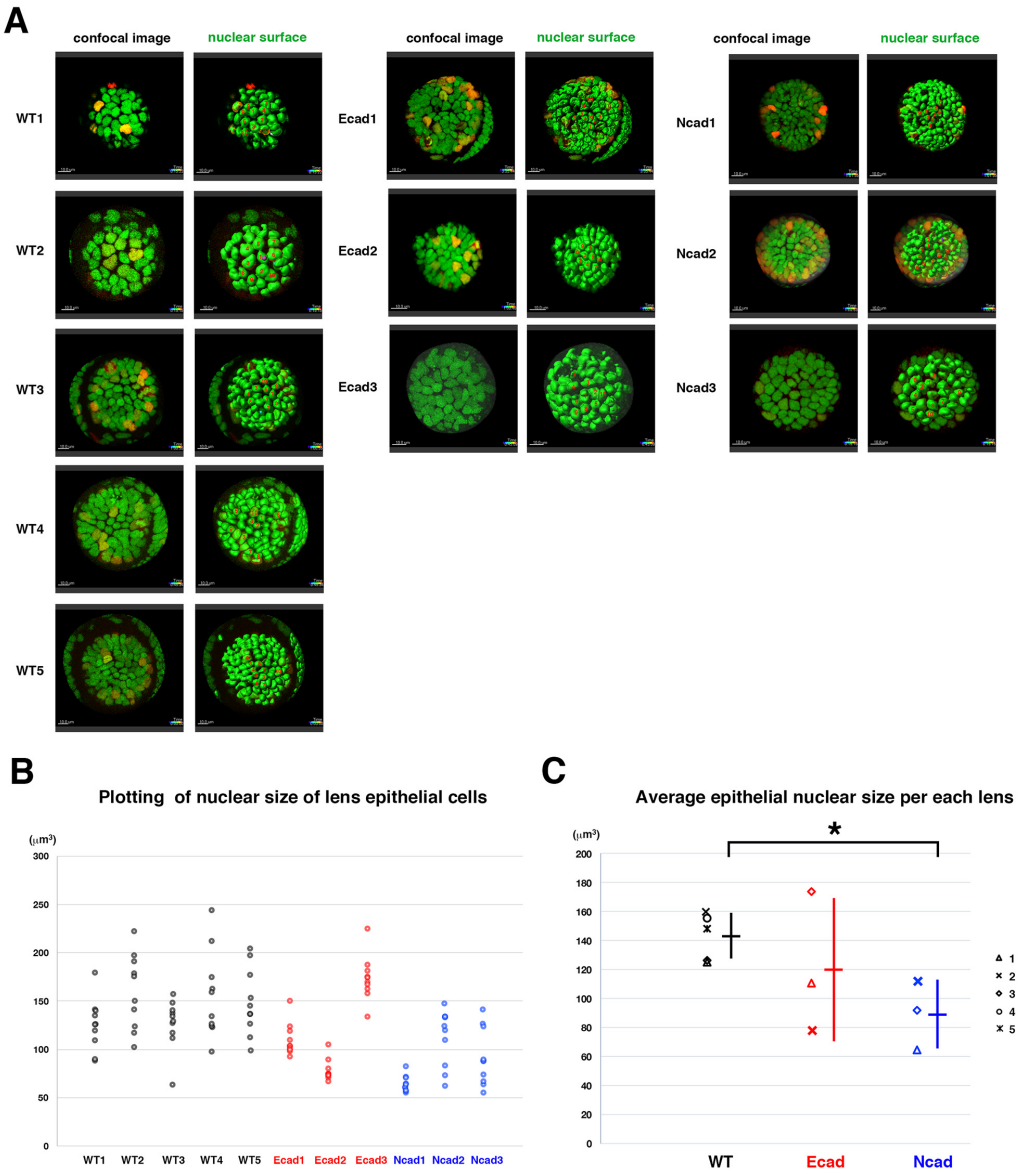

Figure S9. Analyses of nuclear size of lens epithelial cells

(A) Confocal images (left) and surface objects demarcating lens epithelial nucleus (right) in wild-type, E-cadherin mutant, and N-cadherin morphant anterior lens epithelia at an early stage of the scanned period: 33–36 hpf. Ten lens epithelial cell nuclei randomly selected for measurement of nuclear volume are indicated in red in the right panels.

(B) Plotting of nuclear volumes of individual lens epithelial cells per each of wild-type, E-cadherin mutant, and N-cadherin morphant lenses. Distribution range was variable depending on individual lenses, but the range was reduced in E-cad1, E-cad2 and three N-cad lenses and elevated in E-cad3 lenses, compared with wild-type lenses.

(C) Plotting of average nuclear volumes of lens epithelial cells in each lens. Horizontal bars and vertical lines indicate mean and standard deviation of lens epithelial nuclear volume, respectively. Nuclear size of lens epithelial cells was significantly smaller in the N-cadherin morphant than in wild type, whereas the range was broader in the E-cadherin mutant than in wild type. In the N-cadherin morphant, a reduced tensile force and prominent E-cadherin-dependent cell adhesion may reduce nuclear size. In E-cadherin mutant, the absence of adherens junction may weaken the tensile force transmission from plasma membranes to nuclear membranes, resulting in variable nuclear size. Probability is calculated using Student's *t*-text: *p<0.05.

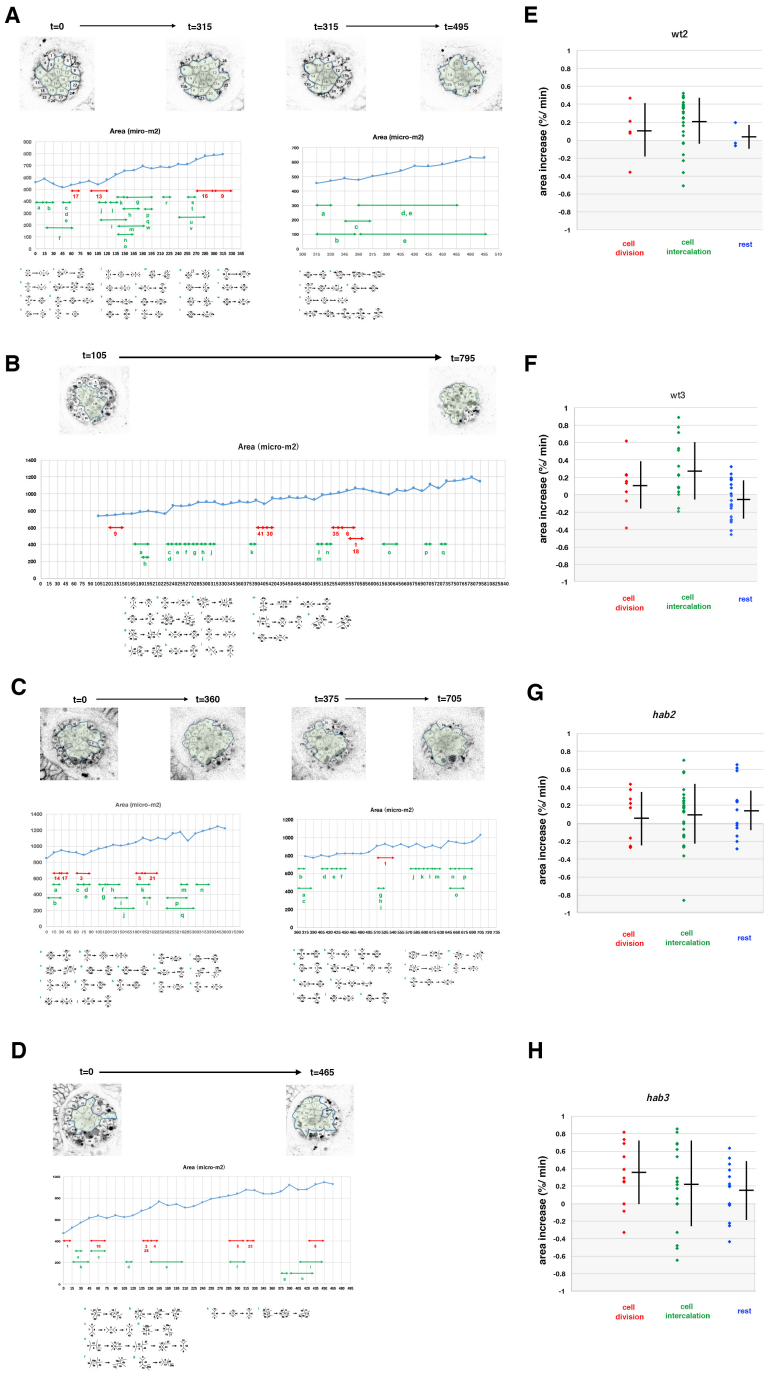

Figure S10. Analyses of lens epithelial expansion of wild-type and E-cadherin mutant lenses

(A, B) Lens epithelial expansion analysis of two wild-type lenses, namely wt2 (A) and wt3 (B). The top panels indicate the composition of individual lens epithelial cells. Middle panels display temporal profiles of the area. Red and green arrows indicate cell division events and periods when cell intercalation occurred, respectively. Bottom panels indicate cell intercalation that occurred in the corresponding period of middle panels.

(C, D) Lens epithelial expansion analysis of two *hab*^{rk3} mutant, namely *hab2* (C) and *hab3* (D).

(E, F) Plotting of expansion rate per each scanned frame (15 min) of two wild-type (A, B) lens epithelial areas during periods of cell division (red), cell intercalation (green), and the rest period without cell division or intercalation (blue). Horizontal bars and vertical lines indicate the mean and standard deviation, respectively.

(G, H) Plotting of expansion rate per each scanned frame (15 min) of two *hab*^{rk3} mutant (C, D) lens epithelial areas during periods of cell division (red), cell intercalation (green), and the rest period without cell division or intercalation (blue). Horizontal bars and vertical lines indicate the mean and standard deviation, respectively.

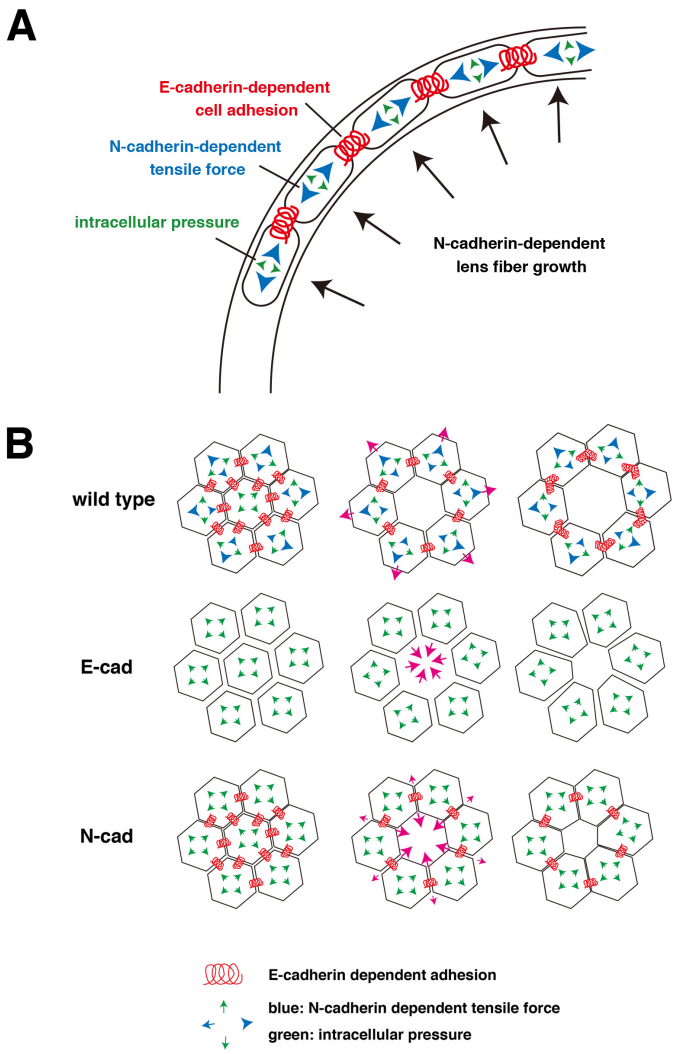

Figure S11. A possible model of lens epithelial forces

(A) N-cadherin promotes lens fiber growth, which increases epithelial tension (blue arrowheads). Force derived from intracellular pressure (green arrowheads) also contributes to the epithelial tension. E-cadherin, a component of adherens junctions (red springs), cooperates with the actomyosin-dependent shrinking force, and counterbalances these tensile forces between epithelial cells.

(B) (Left column) In the wild type, the E-cadherin-mediated cell adhesion force (red springs) counterbalances both the N-cadherin-mediated tensile force (blue arrowheads) and intracellular pressure (green arrowheads) to preserve epithelial tension as elastic energy in the lens epithelium. (Middle column) Removal of a single cell by laser ablation suddenly eliminates the E-cadherin-mediated cell adhesion force between the ablated cell and surrounding cells, resulting in predominance of the tensile force that pulls surrounding cells toward the outside. (Right column) This predominant pulling force induces recoil expansion of the ablated area just after laser ablation. After ~100 second-post ablation, an actomyosin-dependent healing process starts to close the ablated space.

In the E-cadherin mutant, the N-cadherin-mediated tensile force on the lens epithelium is intact. However, since adherens junctions are not absent in the E-cadherin mutant, lens epithelial cells do not sense the N-cadherin-mediated tensile force from neighboring cells. The absence of cell adhesion also increases fluidity of cell movement and flexibility of cell shape in the E-cadherin mutant. After laser ablation, E-cadherin mutant surrounding cells do not expand but passively start to close the ablated space. Since the actomyosin-dependent healing process depends on E-cadherin, the ablated space fails to be closed in the E-cadherin mutant in the later stage. Increased fluidity of cell shape may enlarge the apical size of E-cadherin mutant lens epithelial cells. It is also possible that the reduction of cell division decreases the size of the lens fiber core, which also contributes to reduction of epithelial tension in the E-cadherin mutant.

In the N-cadherin morphant, the N-cadherin-mediated tensile force on the lens epithelium is reduced. The E-cadherin-dependent cell adhesion force counterbalances only the intracellular pressure, which is likely to be less than the normal level of N-cadherin-mediated tensile force in wild type cells. This physical situation weakens the pulling tension preserved in the lens epithelium and shrinks the apical cell size. After laser ablation, surrounding cells do not expand but the ablated area started to close because of the predominant E-cadherin-mediated cell adhesion force between lens epithelial cells.

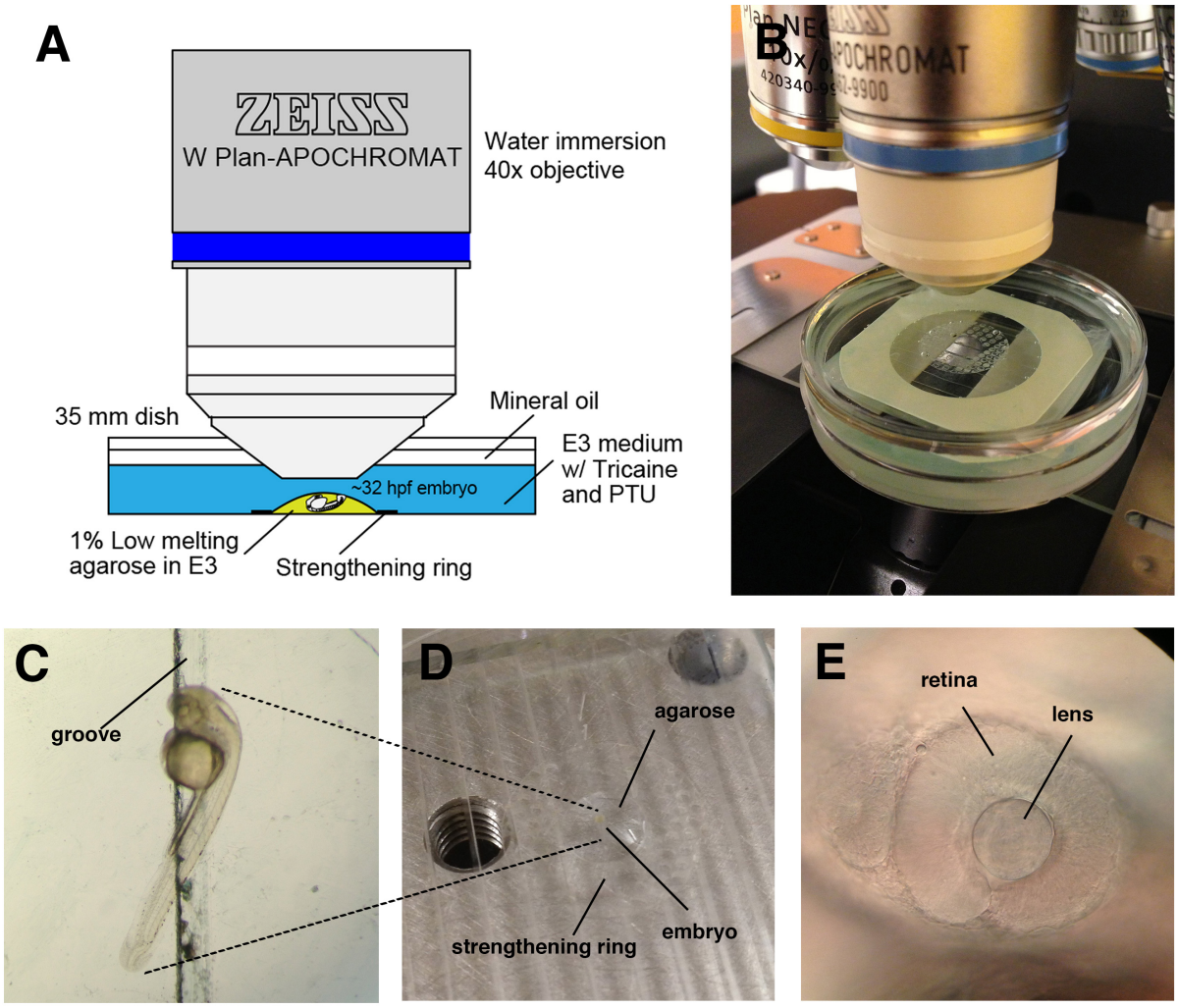

Figure S12. Set-up for time-lapse imaging of zebrafish lens epithelium

(A) Schematic illustration of the imaging setup.

(B) Real set-up picture.

(C) The embryo was mounted in 1% low-melting agarose, and the yolk was put into the groove in order to orient the embryo laterally.

(D) The agarose was restricted within the inner circle of a strengthening ring on the groove stretched into the acrylic plate.

(E) The lateral side of the embryonic eye was used for confocal z-stack scanning.

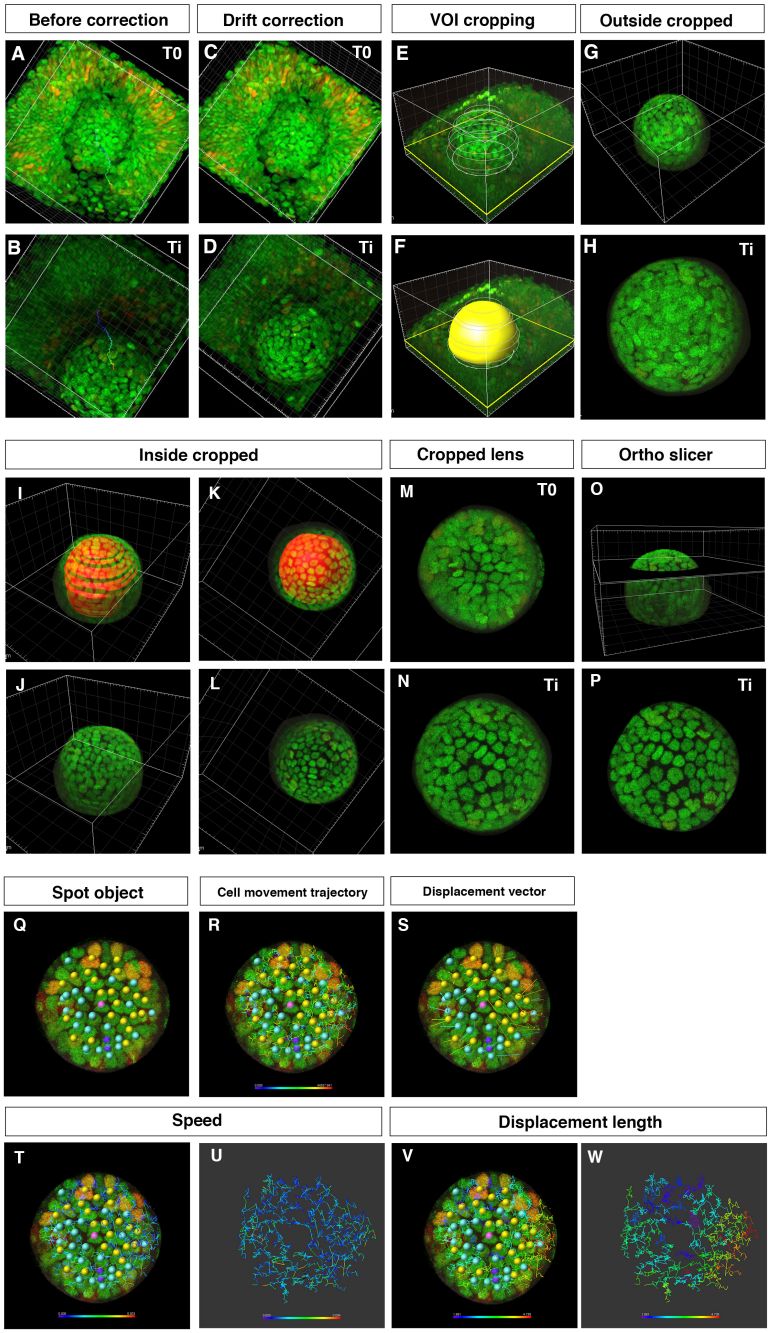

Figure S13. Procedure for obtaining 3D time-lapse images of anterior lens epithelium
(A–D) Two time points from T0 to Ti of embryonic eyes without (A, B) and with drift correction (C, D). (E, F) VOI cropping by drawing outside contour circles and creation of a surface masking the lens. (G, H) Outside cropped lens. (I–L) Cropping of the lens fiber area by drawing inside contour circles and by creating a surface masking the lens fiber area. (M, N) Cropped lens at T0 and Ti. (O, P) Extract of anterior lens epithelium using the "Ortho Slicer" tool. (Q–W) Analysis of cell movement of lens epithelial cells. (Q) Assignment of spot objects to trace cell lineages, which classify epithelial cells into dividing (yellow), non-dividing (blue), and eliminated cell populations (purple). (R) Cell movement trajectory, (S) displacement vector, (T–U) cell movement speed, and (V–W) displacement length.

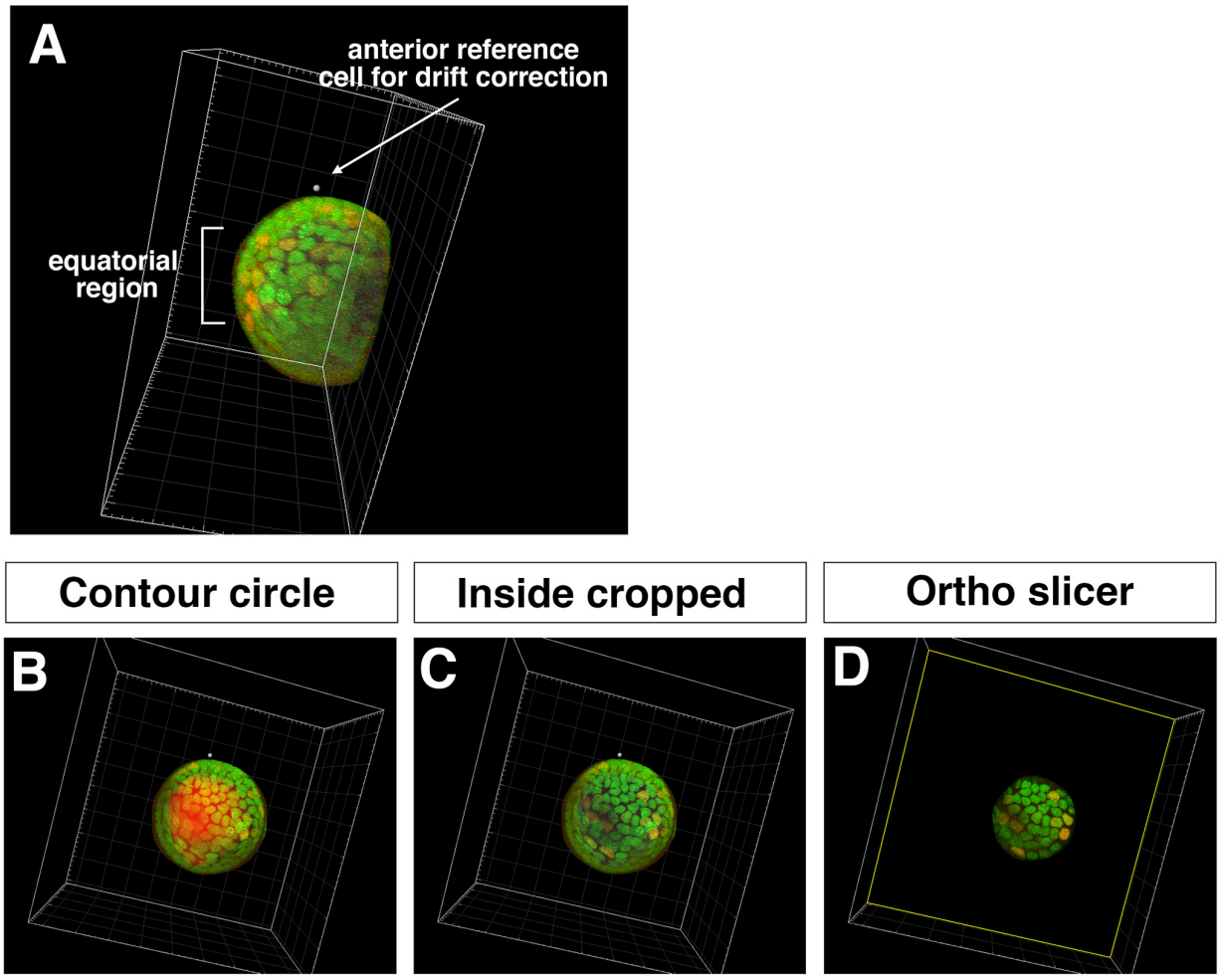

Figure S14. Procedure for obtaining 3D time-lapse images of equatorial lens epithelium

(A) Side view of the lens scanned from the ventral view. Tissues outside the lens sphere, such as the retina and the cornea, were removed by cropping. Anterior reference position used for drift correction and the equatorial region are indicated.

(B) Equatorial view of the lens before cropping the lens fiber core. Contour of the surface masking the lens fiber core is indicated (red).

(C) Equatorial view of the lens after cropping the lens fiber core.

(D) Only the equatorial lens epithelium was extracted using the "Ortho slicer" tool.

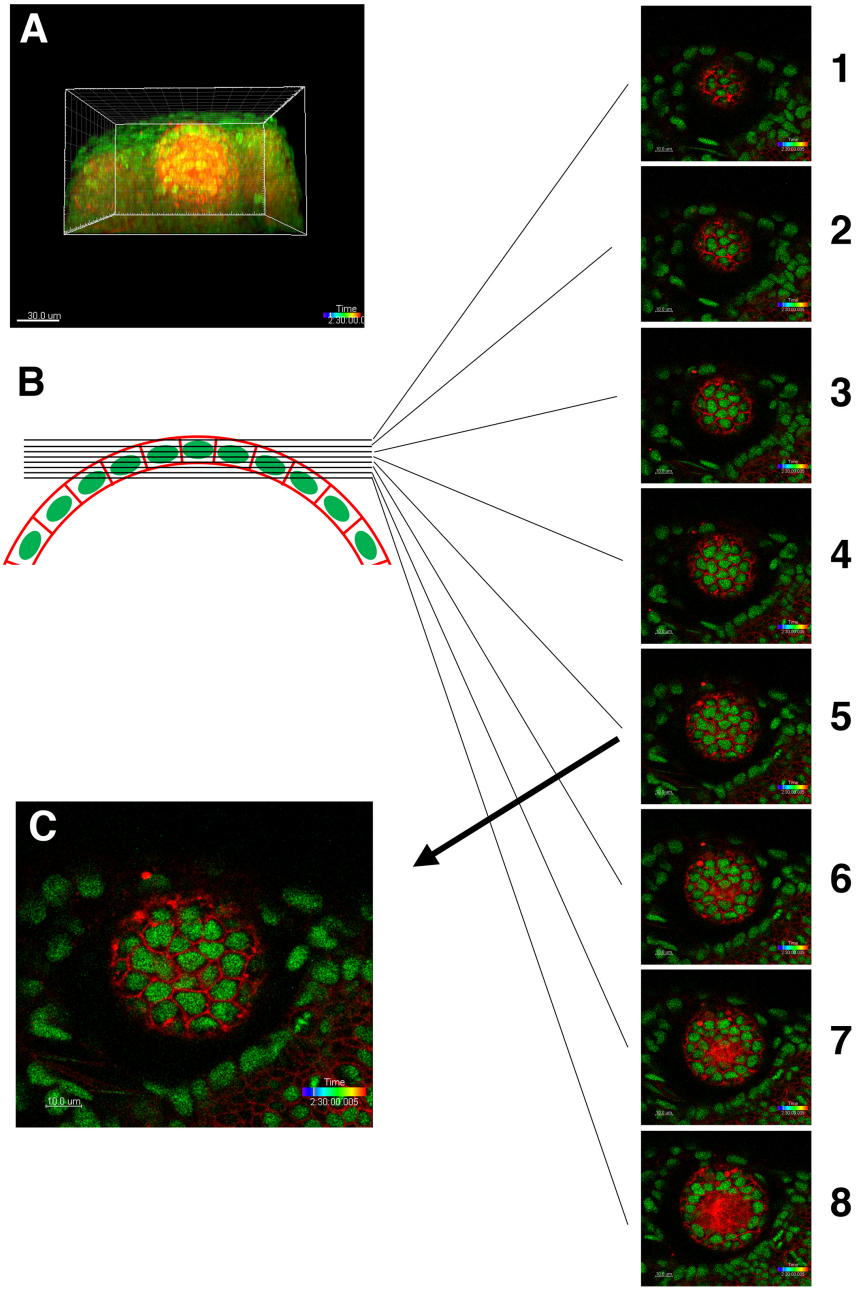

Figure S15. Procedure for selecting a confocal slice of the most apical lens epithelium

(A) 3D confocal image of *Tg(h2afva:GFP; EF1α:mCherry-CAAX)* transgenic fish lens.

(B) Schematic picture of zebrafish lens epithelium and z-axis slice level. Eight slices containing the anterior lens epithelium from the anterior to posterior direction are shown. The interval between neighboring slices is 1 μm. Three posterior slices, #6–8, contains the lens fiber region. Thus, the #5 slice is the most suitable for analysis of cell intercalation and epithelial rearrangement, because CAAX-labeled plasma-membranes correspond to the adherens junction complex-containing domain.

(C) The confocal slice containing the most apical lens epithelium just adjacent to the lens fiber core (indicated as the #5 slice in B), which was used to make a movie and to analyze cell division, cell intercalation, and area expansion.

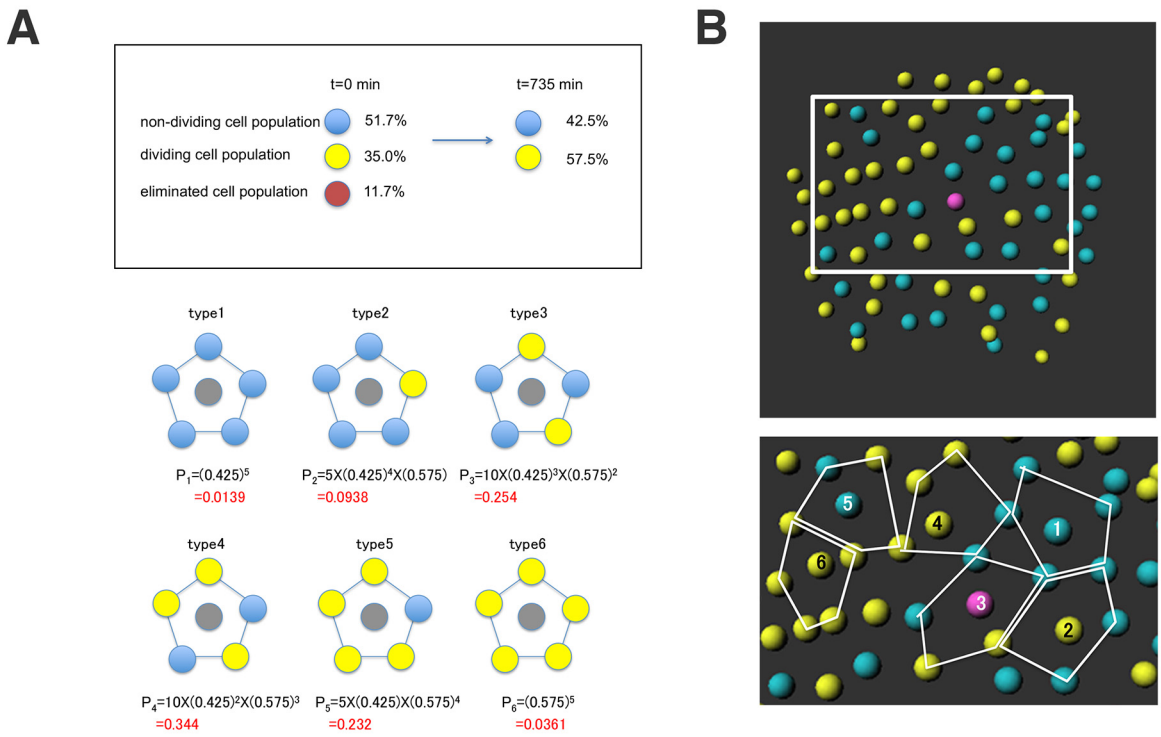

Figure S16. Analyses of non-dividing and dividing cell clusters

(A) Calculation of probability for each pentagonal pattern generated by the random distribution model. In the wild-type lens shown in Figure 1B, non-dividing (blue), dividing (yellow), and eliminated (red) cells comprise 51.7, 35.0, and 11.7% of all cells, respectively, at the beginning of the scanned period (33 hpf). At the end of scanned period (45 hpf), the final ratio of non-dividing and dividing cells is calculated as 42.5 and 57.5%, respectively. Bottom panels indicate six pentagonal patterns depending on combinations of non-dividing (blue) and dividing (yellow) cell populations. On the assumption that non-dividing and dividing cells are distributed at random, the probability for each pattern at 45 hpf is calculated by the equation below.

(B) Example of pentagonal patterns of wild-type lenses shown in Fig. 1B. The number indicates the type of pentagonal pattern.

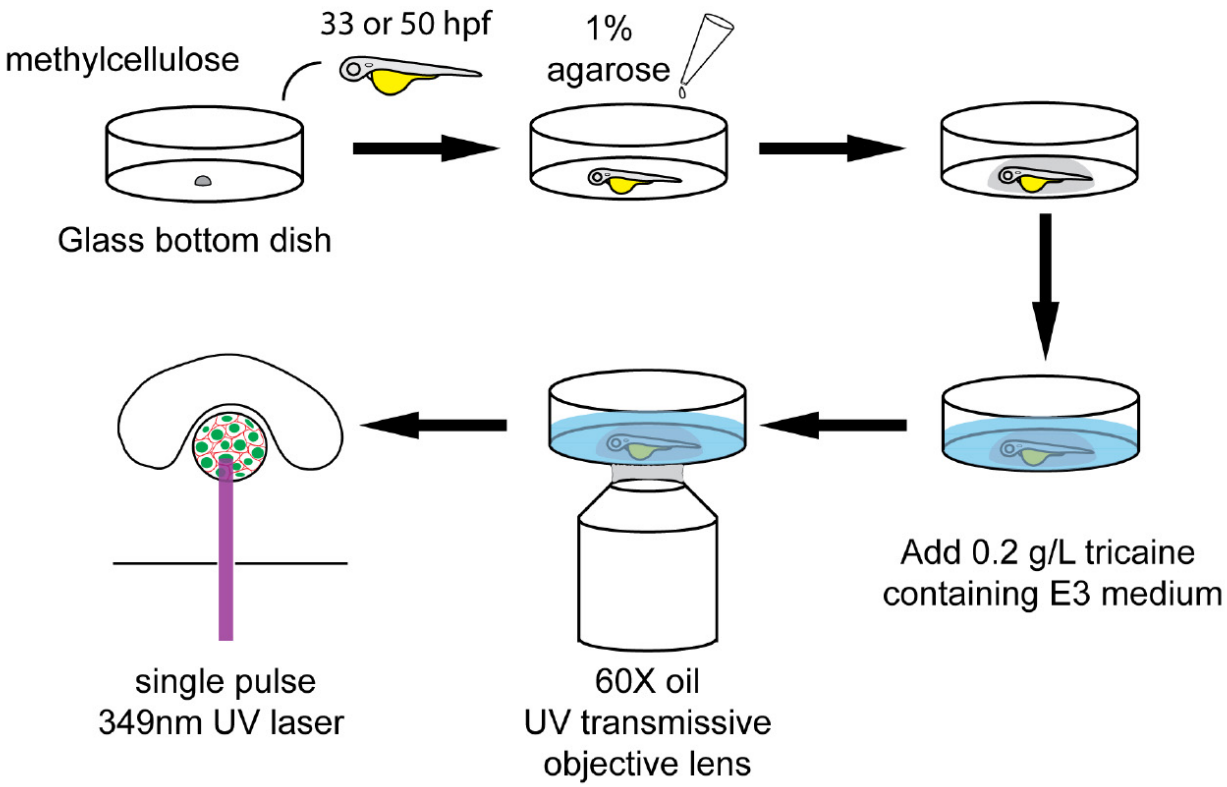

Figure S17. Procedure for mounting zebrafish embryos for laser ablation experiments
Fifty hpf embryos were mounted onto glass-bottom dishes with a drop of 3% methylcellulose, and oriented so that the eye was close to the bottom. Low-melting agarose buffered with E3 medium was then added on top of the embryos to hold the embryo orientation. After solidification of the agarose, E3 medium containing Tricaine was added just before UV laser ablation. After mounting of the dish containing an embryo on the stage of inverted confocal LSM microscope with 60x objective lenses, a single shot of 349nm-UV laser was fired to ablate a single cell of lens epithelium.

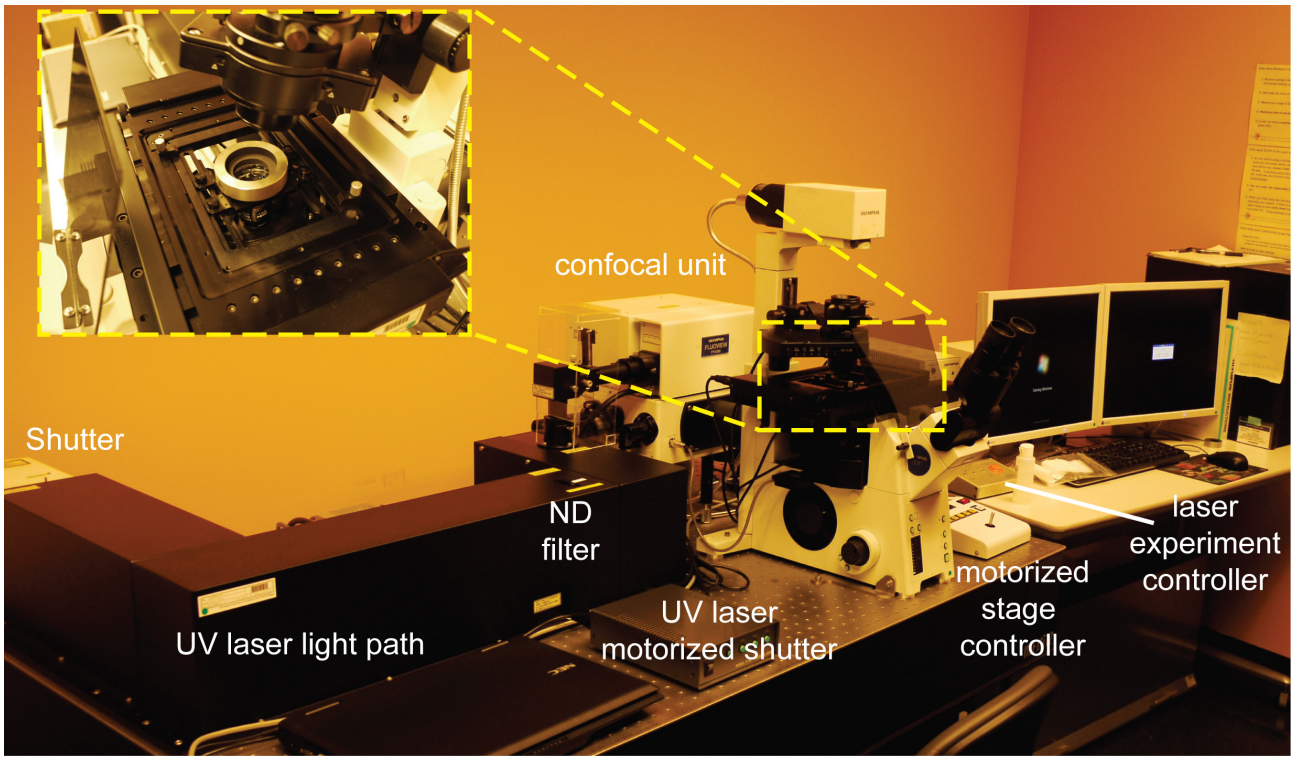

Figure S18. Configuration of the laser ablation system
Confocal laser scanning microscope (the right side of the image, FV1200, Olympus) combined with the UV ablation unit (the left side of the image). Inset indicates mounting of a zebrafish embryo on the stage. A glass dish containing a zebrafish embryo is held to the stage with putting a silver circle metal weight.

A

Laser setting output[%]	UPASAPO60x output[uJ] 20131030 ND 100	ND 50	ND 20	ND 5	ND 1
0					
10					
20					
30	–	–	–	–	–
35	0.21	–	–	–	–
40	0.21	–	–	–	–
45	0.44	0.26	–	–	–
50	0.75	0.42	0.20	–	–
55	1.09	0.61	0.27	–	–
60	1.54	0.83	0.36	–	–
65	2.10	1.13	0.46	–	–
70	2.58	1.39	0.57	0.20	–
75	3.04	1.65	0.66	0.23	–
80	3.58	1.96	0.78	0.26	–
85	4.26	2.31	0.92	0.29	–
90	4.80	2.62	1.05	0.33	–
95	5.40	2.94	1.17	0.36	–
100	5.94	3.23	1.27	0.39	–

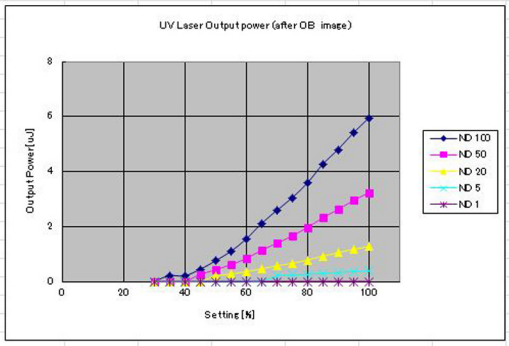

B

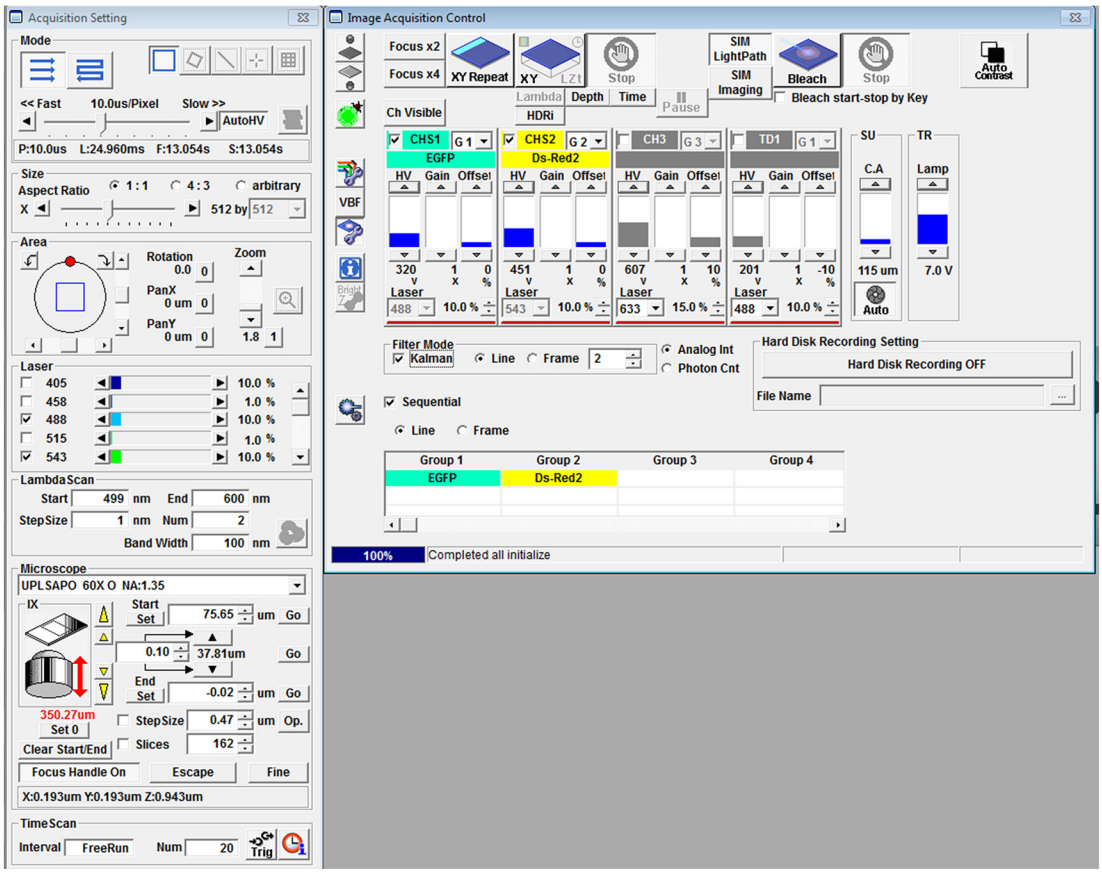

Figure S19. Setting parameters for the laser ablation experiment

(A) The relationship between actual laser power and laser setting output with different neutral density (ND) filter configurations profiled by the manufacturer. We selected 65-80% for laser setting output and an ND50 filter to obtain 1.13-1.96 μJ as the actual laser output at the focal point

(B) Screen shot image of the ablation experiment in FluoView.

Supplementary table I

sample	ND	DV (t=0)	eliminated	Total
WT1	31	21	7	59
WT2	24	19	2	45
WT3	26	21	1	48
WT4	27	12	14	53
WT5	36	16	2	54
E-cad1	43	17	16	76
E-cad2	30	11	5	46
E-cad3	27	8	2	37
N-cad1	30	24	15	69
N-cad2	25	26	3	54
N-cad3	28	18	1	47

Supplementary methods

Time lapse scanning and analysis of *Tg(h2afva:GFP; EF1α:mCherry-zGem) transgenic fish lens*

Zebrafish wild-type, E-cadherin mutant, and N-cadherin morphant embryos carrying the transgene *Tg(h2afva:GFP; EF1α:mCherry-zGem)* were produced and developed by 30 hpf in E3 embryonic medium containing 0.003% 1-phenyl-2-thiourea (PTU), which prevents melanin pigmentation. At 30 hpf, the chorion of embryos was removed, and after anesthetization in 200 mg/L Tricaine (3-amino benzoic acid ethyl ester, Sigma A-5040), embryos were mounted on a microscope stage. Configuration for sample mounting on a confocal laser scanning microscope (LSM) is shown in Fig. S12A–B. Since we used an upright LSM microscope, embryos were mounted on their sides in a groove stretched in an acrylic plate for positioning yolk with a drop of 3% methylene cellulose (Fig. S12C), and covered with 1% low-melting point agarose prepared in E3 medium within a strengthening ring (One-Patch Stamp; Kokuyo, PSM10B; outside diameter, 14.5 mm; inside diameter, 6 mm), which prevents detachment of the agarose from the acryl plate (Fig. S12D). After solidification of the agarose at room temperature, E3 medium with 200 mg/L Tricaine and 0.003% PTU was poured into the dish. Mineral oil was then layered on the E3 medium to prevent evaporation (Fig. S12A–B). Fish embryos were scanned on their sides using a Zeiss LSM confocal system in z-stack and time-series scanning mode (Fig. S12E). General parameters for confocal scanning as followings (Zeiss LSM 710 upright confocal system): Objective, W Plan-Apochromat 40x/1.0 DIC M27; Resolution, 512x512 pixels in 8-bit; Pinhole, 40–70 μm; Scanning mode, bidirectional and speed 6-7; Noise reduction, line 2 scan in median mode; Laser power, 488 nm 3–4%, 543 nm 10%; Master gain 1000–1100V; Digital Gain, 1.0; Digital offset, -10; Zoom, 1.0–1.3.

For time-lapse scanning with the confocal LSM, the region of interest of lens was first cropped using Zeiss imaging software, ZEN, to reduce the file size. Noise was reduced using a median filter. Time-lapse images were obtained every 15 min for 12 hr after 33 hpf. Scanned 3D time-lapse movies were analyzed with Imaris software (ver. 7.6.5, Bitplane). Drifting lens position during the scanned period was corrected using the "Drift Correction" tool of Imaris software, which selected one nucleus that showed no cell division and little or no movement within the most anterior area, as a steady-point reference and adjusted surrounding images relative to this reference (Fig. S13A–D). The volume of interest (VOI) of the lens was then cropped by drawing contour circles and by creating a surface that masked the lens (Fig. S13E–H). Next, the internal lens fiber area was cropped by drawing inside contour circles and by creating a surface that masked the lens fiber core (Fig. S13I–L). Throughout these processes, digitally resected lens epithelium was prepared (Fig. S13M–N), and its anterior lens epithelium was further extracted using Imaris "Ortho Slicer" tool (Fig. S13O–P) and used for epithelial cell movement tracking and behavior analysis.

After we obtained 3D time-lapse movies of five wild-type, three E-cadherin mutant, and three N-cadherin morphant lenses, cell lineages for each lens were traced with connecting nuclei between individual time-lapse images using the Imaris "Track Particles" tool with manual

correction (Fig. S13Q–S). All epithelial cells were classified as dividing, non-dividing and eliminated cell populations for each lens (Supplementary Table I), and the eliminated cell population was further classified into cells that underwent apoptosis or that simply moved out of the lens epithelium by monitoring whether chromatin collapsed when eliminated cell population disappeared, and these data were analyzed to calculate the fraction of these cell populations for each genotype (Fig. S1A–D and Fig. S2A). Next, using cell lineage data, cell movement speed, tracking length, and displacement length for each time frame were measured for each lineage of dividing and non-dividing cell population: especially, for dividing cell population, two daughter cell lineages were separately analyzed, and shown on trajectory maps (Fig. S13T–W). Average values of these parameters during the scanned period were calculated for each cell lineage from the Imaris Dataset, and average values of cell movement speed, tracking length, and displacement length for dividing and non-dividing cell populations were calculated for each lens using average values of each cell lineage. For analyses of cell movement parameters in cell-cycle phases, speed of cell movement on each time frame was manually calculated using cell position distance between the preceding and immediately following time frames. Cell-cycle phases of individual cells for each time frame were determined by fluorescent colors of *Tg(h2afva:GFP; EF1α:mCherry-zGem)*. Combined with this information, average speed of cells in G1, S/G2, and M phase were calculated for each lens.

For measurement of nuclear volume, objects demarcating the surface of GFP-labeled chromatin in the anterior lens epithelium were created for individual time-lapse movies, using the "surface rendering" tool of the Imaris software (Fig. S9A), and their volume were calculated. Ten lens epithelial cells were selected in the early stage of the scanned period (33–36 hpf) when no apoptotic cells were observed. The average value of epithelial nuclear volume was calculated using these ten samples for each lens (Fig. S9B). Five wild-type, three E-cadherin mutant, and three N-cadherin morphant lenses were used for evaluation of the difference in lens epithelial nuclear size for each genotype (Fig. S9C).

For time-lapse scanning of the equatorial region of the lens, the same time-lapse scanning procedure for the anterior lens epithelium was applied, except that embryos were mounted in a ventral view on a groove stretched in an acrylic plate. Drift movement was corrected using the most anterior lens epithelial cell that showed no cell division and little or no movement, as a steady-point reference and the lens was extracted by cropping the outside retina and cornea (Fig. S14A). Then, lens epithelium in the equatorial region was digitally resected by cropping the inside lens fiber cores (Fig. S14B–C) and using "Ortho slicer" tool (Fig. S14D).

Time lapse scanning and analysis of *Tg(h2afva:GFP; EF1α:mCherry-CAAX)* transgenic fish lens

Zebrafish wild-type and E-cadherin mutant embryos carrying the transgene *Tg(h2afva:GFP; EF1α:mCherry-CAAX)* were produced and developed by 30 hpf in E3 embryonic medium containing 0.003% PTU. Time-lapse images of the anterior lens epithelium from *Tg(h2afva:GFP;*

EF1α:mCherry-CAAX) fish were obtained using the same procedure as with *Tg(h2afva:GFP; EF1α:mCherry-zGem)* fish (Fig. S15A). After correcting for drift during scanning, the lens epithelium was cropped by drawing outer contours and by performing surface masking. The major reason for using *Tg(h2afva:GFP; EF1α:mCherry-CAAX)* was to obtain the information on the plasma membrane domain that is associated with adherens junctions for analyses of epithelial cell arrangement, such as cell intercalation. The most anterior region of lens epithelium usually consists of around eight confocal slices 1 μm thick along the AP axis, and among these eight slices, only one corresponds to the focal plane, which contains a plasma membrane domain that is associated with adherens junctions and is just adjacent to the anterior top of lens fiber core (Fig. S15B). Thus, we extracted such confocal images from a series of 3D z-axis stacked images using the "Ortho Slicer" tool or by selecting an appropriate confocal image slice for each of 15 min time point (Fig. S15C) and compiling them to make a time-lapse movie. Since the movie provides information on plasma membranes associated with adherens junctions, it is useful for studying cell intercalation. Individual cell lineages were traced with assignment identification numbers for each cell throughout the scanned period.

For evaluation of lens epithelial area expansion during development, we selected 10-15 cells in movies of the apical lens epithelial region for three wild-type and three *hab*^{rk3} mutant lenses, and calculated cell areas at each time point, using ImageJ. We also manually identified cell divisions and cell intercalations in each movie and examined temporal relationships between cell division and cell intercalation. Area expansion rate for each 15 min interval (% of original area size/min) was calculated. The average expansion rate was calculated for cell division period, cell intercalation period, and for the rest period when cell division and cell intercalation do not occur.

Determination of cell movement direction

Cell movement direction in the lens epithelium was calculated using time-lapse 3D images from an anterior view. In XYZ coordinates of time-lapse images after drift correction, the position of the reference nucleus, which corresponds to the anterior pole of the lens sphere, is defined as (0, 0, 0). When an epithelial cell (nucleus) moved from position (x_1, y_1, z_1) to (x_2, y_2, z_2) in the lens epithelium, the displacement vector X (x_d, y_d, z_d) was determined using the following equations: $x_d = x_2 - x_1$; $y_d = y_2 - y_1$; $z_d = z_2 - z_1$. We defined cell movement direction as the angle θ between the line from (x_1, y_1, z_1) to (x_2, y_2, z_2) and the circumferential line that crosses the initial cell position (x_1, y_1, z_1). To calculate θ, we defined vector A (a, b, 0) that is parallel to the circumferential line that crosses the initial cell position (x_1, y_1, z_1). The vector A (a, b, 0) should be perpendicular to a vector (x_1, y_1, 0) and calculated using the equation shown below (where $a^2+b^2=1$).

$$A(a, b, 0) = \left(\frac{y_1}{\sqrt{{x_1}^2 + {y_1}^2}}, \frac{x_1}{\sqrt{{x_1}^2 + {y_1}^2}}, 0\right)$$

Whereas θ is calculated using the equation below.

$$\cos\theta = \frac{|ax_d + by_d|}{|\vec{A}||\vec{X}|}$$

To determine cell movement direction along the AP axis, lens epithelial region was divided into sub-regions along the AP axis: r=0–6, 6–11, 11–16, 16–21, 21–26, 26–31 (μm). Lens epithelial cells positioned in each sub-region at the beginning of the scanned period (t=0) were identified and their displacement vectors from t=0 to t=735 min were determined. The vector A was also determined for each lens epithelial cell. Then, cell movement orientation θ was calculated using the equation above. The average of cell movement orientation θ was determined per sub-region of the AP axis in wild-type, E-cadherin mutant and N-cadherin morphant lenses and was plotted in the histograms shown in Fig. 1H, 3F and 4F, respectively.

The cell movement angle in the equatorial region was also defined as the angle between the displacement vector and the circumferential axis. In both cases, 0° was defined as circumferential movement and –90° as longitudinal movement toward the posterior pole.

Evaluation of cell clustering

We conducted cell clustering analyses at three time points during the scanned period: t=0, 360, and 735 min elapsed after 33 hpf. First, we determined the number of non-dividing, dividing and eliminated cell populations, which are defined as $N(t)_{ND}$, $N(t)_{DV}$, and $N(t)_e$, respectively, at the three time points in wild-type, E-cadherin mutant and N-cadherin morphant lenses. During the time-lapse scanning period (33–45 hpf), the eliminated cell population disappeared, whereas the dividing cell population doubled during one round of cell division. In accordance with our definition, cells that had not divided, but would undergo cell division later were pre-designated as belonging to dividing cell population even before the actual time of cell division. Similarly, cells that had not disappeared, but would be eliminated later were pre-designated as members of eliminated cell population before their actual time of cell elimination. Since almost all eliminated cells we observed in this analysis did not divide during scanning, we counted eliminated cell population as non-dividing cell population at t=0 and 360 for the classification of pentagonal cell cluster patterns. To determine the distribution pattern of pentagonal cell clusters in the random distribution model, we calculated the ratio of the number of non-dividing and dividing cell populations relative to total lens epithelial cells at each time point (t), $R_{ND}(t)$ and $R_{DV}(t)$, using the following equations.

$$\mathrm{R}(t)_{ND} = \frac{\mathrm{N}(t=33)_{ND} + \mathrm{N}(t)_e}{\mathrm{N}(t=33)_{ND} + \mathrm{N}(t)_e + \mathrm{N}(t)_{DV}}$$

$$\mathrm{R}(t)_{DV} = \frac{\mathrm{N}(t)_{DV}}{\mathrm{N}(t=33)_{ND} + \mathrm{N}(t)_e + \mathrm{N}(t)_{DV}}$$

Using images of *Tg(h2afva:GFP)*, we selected the five cells closest to the cell of interest, forming a virtual pentagon of surrounding cells. Pentagonal cell patterns are classified into six types depending on combinations of dividing and non-dividing cell numbers: type 1 (all 5 non-dividing cells), type 2 (4 non-dividing cells and 1 dividing cell), type 3 (3 non-dividing and 2 dividing cells), type 4 (2 non-dividing and 3 dividing cells), type 5 (1 non-dividing and 4 dividing cells) and type 6 (all 5 dividing cells). The probability of type n when a pentagonal pattern is generated by the random distribution, P_n, was calculated from the equation below.

$$P_n = C_{n-1}^{5} \times \mathrm{R}(t)_{ND}{}^{6-n} \times \mathrm{R}(t)_{DV}{}^{n-1}$$

The procedure for calculating the probability for each pentagonal pattern of a wild-type lens WT1 at 45 hpf was indicated as an example in Fig. S16A.

Next, to determine the distributional profile of dividing and non-dividing cell populations, we examined the pentagonal patterns of individual lens epithelial cells using schematic images representing non-dividing, dividing and eliminated cell populations as blue, yellow, and purple respectively (Fig. S16B), and determined the distribution profile of non-dividing and dividing cell populations. Distribution profiles of pentagonal clusters with a centered dividing cell population and a centered non-dividing cell population, and of the random distribution model are shown in the middle panel of Fig. 1E (WT1, t=735 min), the top panels of Fig. 3C (E-cad1, t=735 min) and Fig. 4C (N-cad1, t=735 min), and Fig. S3A (WT1~5, E-cad1~3, and N-cad1~3; t=0, 360 and 735 min). The average number of dividing cell population in pentagonal clusters for each lens and for each genotype was calculated and shown in Fig. S3B and S3C, respectively.

Laser ablation experiments

Zebrafish wild-type and E-cadherin mutant embryos carrying the transgene *Tg(h2afva:GFP; EF1α:mCherry-CAAX)* were produced and developed by 50 hpf in E3 embryonic medium containing 0.003% PTU. N-cadherin morphant embryos carrying the transgene *Tg(h2afva:GFP; EF1α:mCherry-CAAX)* were prepared by injection of MO-Ncad at 50 μM. At 50 hpf, embryonic chorions were removed and embryos were anesthetized in E3 embryonic medium containing 200 mg/L Tricaine. Embryos were mounted onto glass-bottom dishes (diameter 27mm, 3910-035, IWAKI, Japan) with a drop of 3% methylcellulose (M-0387, Sigma-Aldrich, USA), and oriented so that the eye was close to the bottom. 50 μL of 1.3% low-melting agarose buffered with E3 medium at 42 ºC was then added on top of the embryos to hold the embryo orientation. After solidification of the agarose, E3 medium containing Tricaine was added just before UV laser ablation. The workflow is shown in Fig. S17.

The UV laser ablation unit was combined with an inverted confocal laser scanning microscope (FV1200 on IX81 motorized microscope, Olympus, Japan) (Fig. S18). The UV laser unit was based on a solid-state, Q-switched, 349-nm UV laser with pulse width (FWHM) <5ns,

adjustable repetition rate up to 5 kHz, and maximum power up to 20 μJ (Explorer OEM, Explorer-349-120-1KE, Nd:YLF gain medium, Spectral Physics, USA). The microscope objective lens with high UV transmission (UPlanSAPO 60X Oil, NA=1.35, ∞/0.17/FN26.5, Olympus, Japan) was used. A glass bottom dish with a mounted fish embryo was put on the stage and held firmly by a weight (JA710800, Olympus) as shown in the inset of Fig. S18. The embryo was moved into the center of the view field so that the lens epithelial cell to be ablated was centered. A single laser shot with just enough power for single cell ablation was fired during the first few frames of time-lapse scanning of lens epithelium. In accordance with information on the relationship between actual laser power and laser setting output provided by the company (Fig. S19A), a Neural Density 50 (ND50) filter was used for all experiments. Laser output was set between 65-80%, so that the actual laser output at the focal point was 1.13-1.96 μJ. Parameters for the confocal microscope were as follows.

(1) Scanning speed: 10 μm/pixel
(2) Resolution: 512x512 pixels
(3) Magnification: 1.8X
(4) 488 nm & 543 nm laser power: 10%
(5) Gain: 1X
(6) Kalman Filter:2
(7) Sequential line scanning
(8) Without differential interference contrast
(9) Acquisition interval: 15 seconds

Screenshot pf the ablation experiment in FluoView of FV1200 is shown in Fig. S19B.
Using ImageJ software, the ablated area was analyzed.

Movies

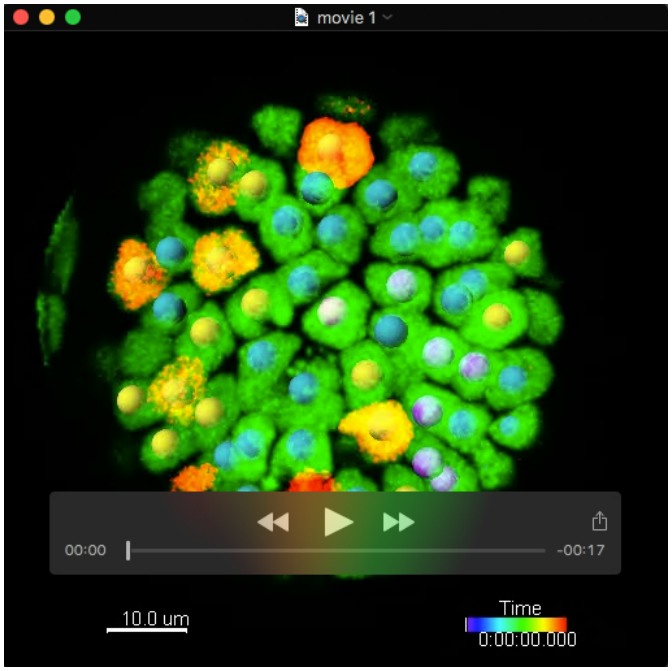

Movie 1

Time-lapse movie of the anterior region of wild-type lens epithelium combined with a zebrafish transgenic line *Tg(h2afva:GFP; EF1α:mCherry-zGem)* from 33 to 45 hpf. Green and red fluorescence indicates cells undergoing the G1 and the S/G2/M phase, respectively. In M phase, chromatin labeled in green fluorescence is condensed. Movie images are associated with spot representation, in which dividing, non-dividing, and eliminated cell populations are indicated by yellow, blue, and purple, respectively. Spot colors are based on the rule by which dividing and eliminated cells were marked beforehand, prior to cell division and cell elimination, respectively.

Movie 2

Time-lapse movie of the most apical region of wild-type lens epithelium combined with a zebrafish transgenic line *Tg(h2afva:GFP; EF1α:mCherry-CAAX)* from 33 to 45 hpf.

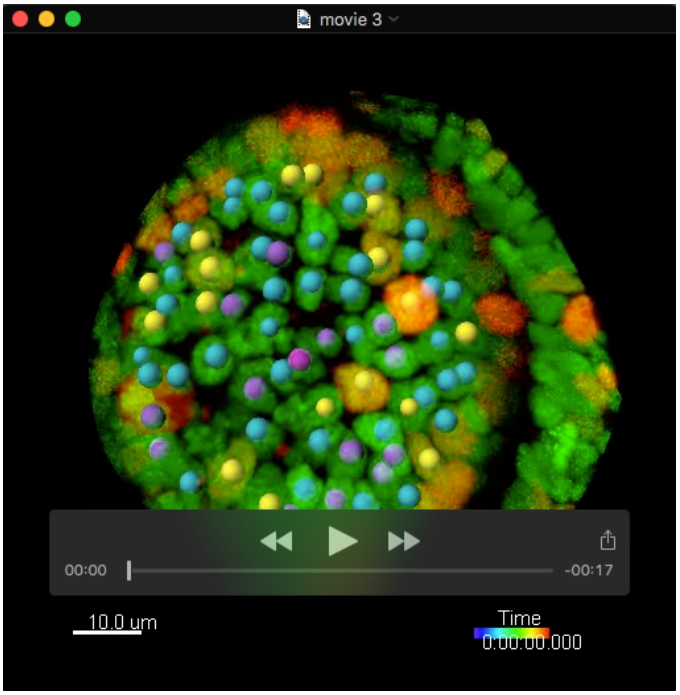

Movie 3

Time-lapse movie of the anterior region of E-cadherin mutant lens epithelium combined with a zebrafish transgenic line *Tg(h2afva:GFP; EF1α:mCherry-zGem)* from 33 to 45 hpf. Movie images are associated with spot representation, in which dividing, non-dividing, and eliminated cell populations are indicated by yellow, blue, and purple, respectively.

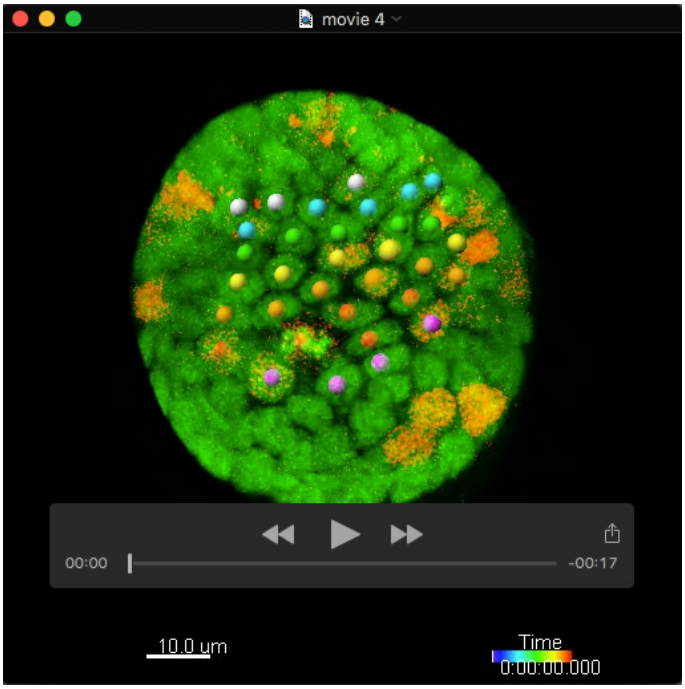

Movie 4

Time-lapse movie of the equatorial region of wild-type lens epithelium combined with a zebrafish transgenic line, *Tg(h2afva:GFP; EF1α:mCherry-zGem)* from 33 to 45 hpf. Different cell rows are indicated by color: Row 0, white; Row 1, light blue; Row 2, green; Row 3, yellow; Row 4, orange; Row 5, red; and Row 6, pink.

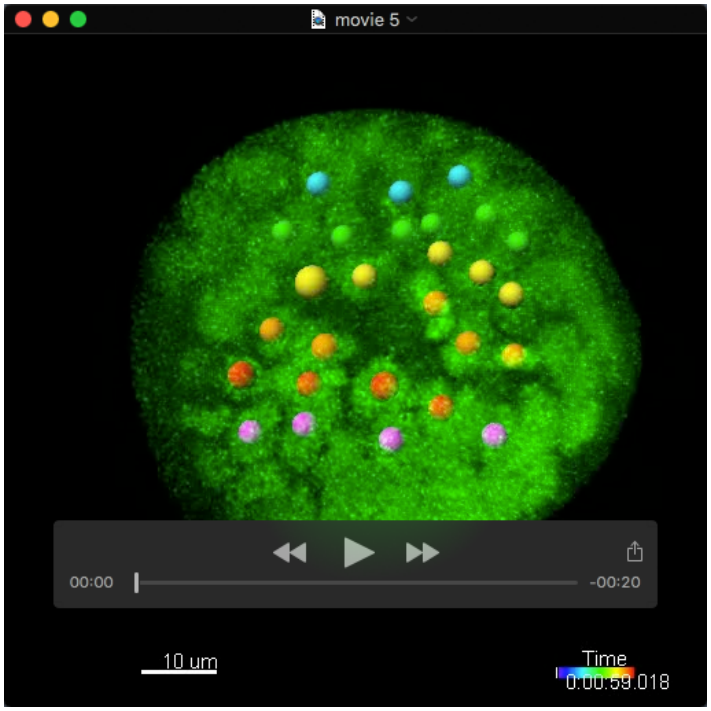

Movie 5

Time-lapse movie of the equatorial region of E-cadherin mutant lens epithelium combined with a zebrafish transgenic line, *Tg(h2afva:GFP)* from 33 to 45 hpf. Different rows of cells are indicated by color: Row 1, light blue; Row 2, green; Row 3, yellow; Row 4, orange; Row 5, red; Row 6, pink.

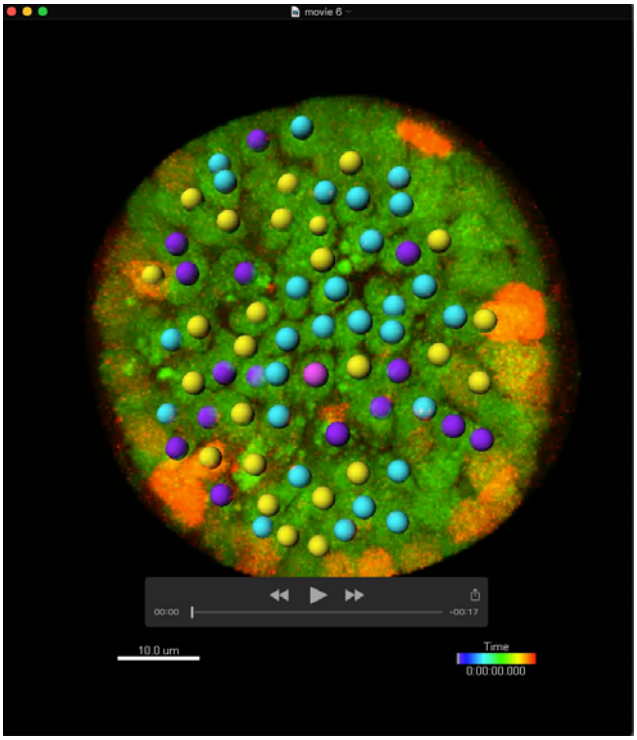

Movie 6

Time-lapse movie of the anterior region of *N-cadherin* morphant lens epithelium combined with a zebrafish transgenic line *Tg(h2afva:GFP; EF1α:mCherry-zGem)* from 33 to 45 hpf. Movie images are associated with spot representation, in which dividing, non-dividing, and eliminated cell populations are indicated by yellow, blue, and purple, respectively.

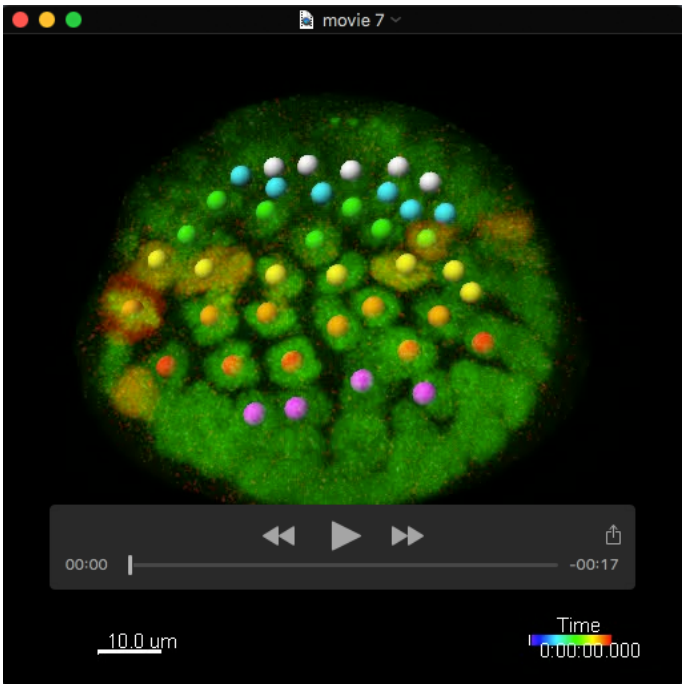

Movie 7

Time-lapse movie of the equatorial region of an *N-cadherin* morphant lens epithelium combined with a zebrafish transgenic line *Tg(h2afva:GFP; EF1α:mCherry-zGem)* from 33 to 45 hpf. Different rows of cells are indicated by color: Row 0, white; Row 1, light blue; Row 2, green; Row 3, yellow; Row 4, orange; Row 5, red; and Row 6, pink.

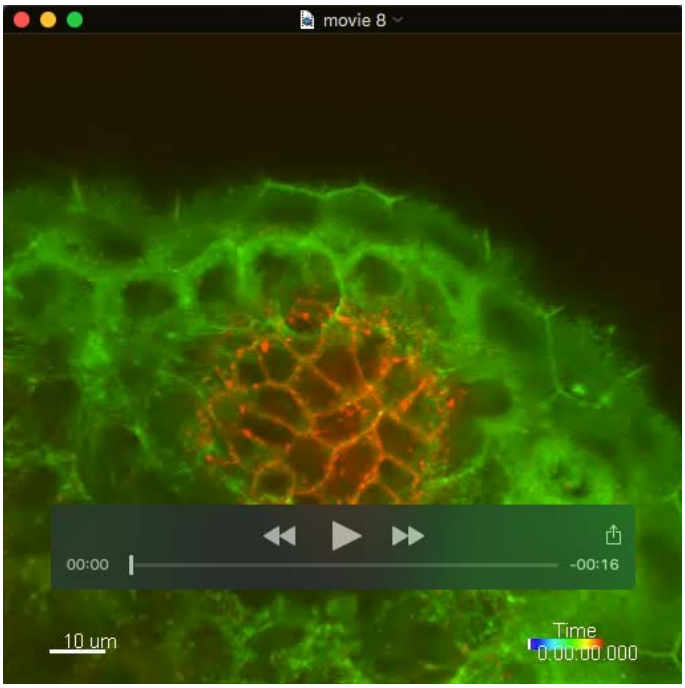

Movie 8

Time-lapse movie of the anterior region of 50 hpf wild-type lens epithelium combined with a zebrafish transgenic line, *Tg(actb1:myl12.1-eGFP; EF1α:mCherry-CAAX)* after the laser ablation.

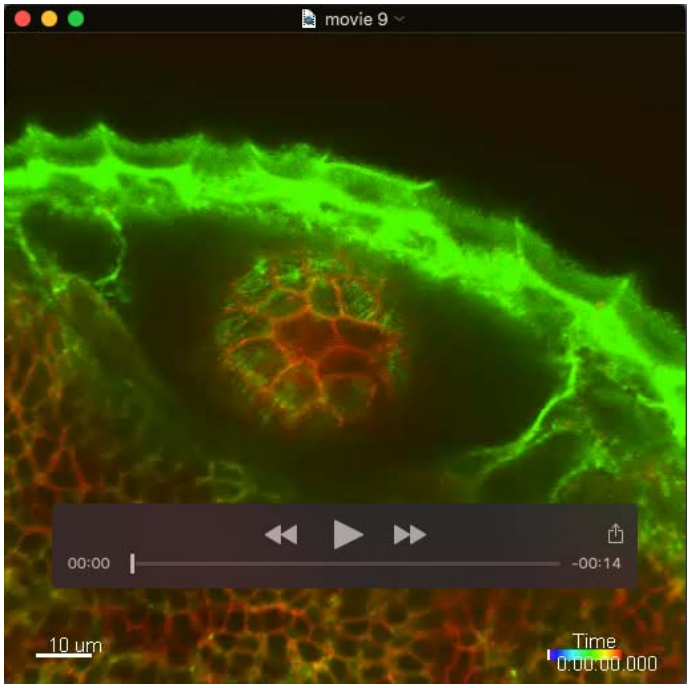

Movie 9

Time-lapse movie of the anterior region of 50 hpf *E-cadherin* morphant lens epithelium combined with a zebrafish transgenic line, *Tg(actb1:myl12.1-eGFP; EF1α:mCherry-CAAX)* after laser ablation.

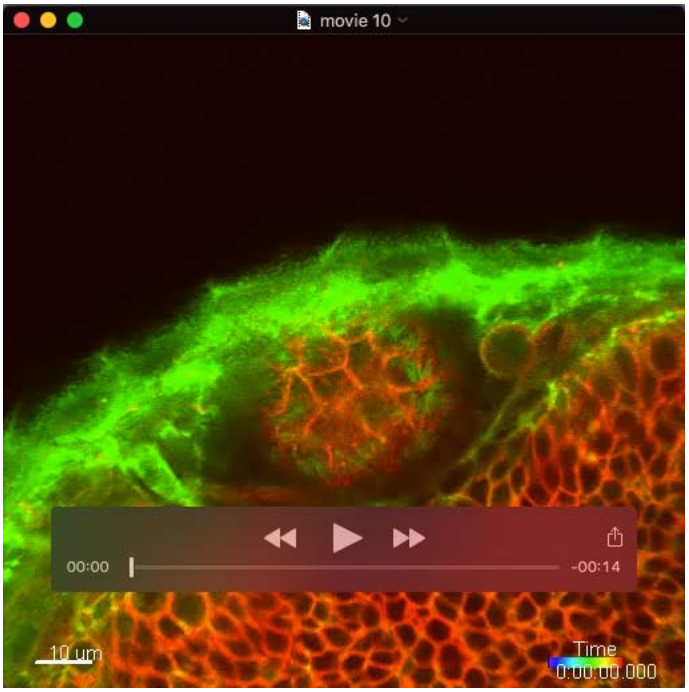

Movie 10

Time-lapse movie of the anterior region of 50 hpf *N-cadherin* morphant lens epithelium combined with a zebrafish transgenic line, *Tg(actb1:myl12.1-eGFP; EF1α:mCherry-CAAX)* after laser ablation.